Supplementary Information for

A 20 million-year Great Ediacaran Glaciation witnessed the rise of the earliest animals

Correspondence to: B. Shen (bingshen@pku.edu.cn), X. Lang (langxianguo19@cdut.edu.cn), B. Wen (wenbin@cug.edu.cn)

This PDF file includes:

Supplementary Text
Figs. S1 to S9
Tables S1 to S5

Supplementary Text

1. Geological setting and section description

The Neoproterozoic succession in the Quruqtagh area, Tarim Block (Fig.S1), i.e., the Quruqtagh Group, is composed of, in the ascending order, the Beiyixi, Zhaobishan, Aletonggou, Tereeken, Zhamoketi, Yukengou, Shuiquan and Hankalchough formations. The total thickness of the Quruqtagh Group is >2700m (Xu et al., 2005). The Beiyixi, Tereeken and Hankalchough formations are mainly composed of diamictite, pebbly sandstone, and intercalated siltstone and sandstone, and represent three glacial intervals, in chronological order, the Beiyixi, Tereeken, and Hankalchough glaciations (Shen et al., 2011). The Beiyixi glaciation was dated between 740 ± 7 Ma and 725 ± 10 Ma (Xu et al., 2009). The Tereeken Formation underlies a 5-10 m-thick cap carbonate in the basal Zhamoketi Formation (Xiao, 2004), which was proposed to be correlated with the Marinoan cap carbonate, and thus the Tereeken glaciation may be equivalent to the Marinoan glaciation. Such correlation is consistent with a zircon U-Pb age of 615 ± 6 Ma from the overlying Zhamoketi Formation (Xu et al., 2009). The Hankalchough Formation conformably overlies the Shuiquan Formation and unconformably underlies the early Cambrian Xishanblac Formation. Therefore, the Hankalchough glaciation was an Ediacaran glaciation in the Tarim Block.

At the Mochia-Khutuk section (MK, 41°26 '29 "N, 87°51' 47" E), the Shuiquan Formation conformably overlies the dark gray siltstone/mudstone of the Yukengou Formation, and is divided into five lithological units (Fig. S2). The unit 1 (U1) consists of intercalated thin-bedded microcrystalline limestone and shale at the bottom and the reddish thin- to medium-bedded coarse crystalline dolostone at the top. The unit 2 (U2) is composed of medium- to thick-bed laminated limestone. The overlying unit 3 (U3) is characterized by limestone-marl alternations that consist of alternating depositions of cm-thick reddish-brown marlstone and light-gray limestone layers. The unit 4 (U4) is composed of thin-bedded limestone with some degree of silicification. The top of Shuiquan Formation (U5) is mainly composed of black calcareous siltstone intercalated with thin-bedded lime mudstone layers.

In the Heishan-Zhaobishan section (HZ, 41°28 '18.6 "N, 88°18' 14.5" E), the Shuiquan Formation can also be divided into five lithological members (Figs. S2 and S3), in stratigraphic order, the reddish-brown dolostone member with limestone layers at the top (M1, 5 m), the limestone-marl alternations member (M2, 10 m), the thin-bedded limestone member with occasional occurrences of shale beds (M3, 78 m), the shale-calcareous siltstone member (M4, 12 m), and the upper thin-bedded limestone member (M5, 5 m).

The MK carbonate may deposit in shallower water than the HZ section. This interpretation is mainly supported by the following sedimentological evidence. (1) The overlying Hankalchough diamictite thickens eastward from ~50 m to ~400 m, indicating deeper basin and more accommodation to the east (Gao and Zhu, 1984). (2) In the overlying Hankalchough cap carbonate, the siliciclastic size and content decreases from west to east, suggesting the eastward transport of siliciclasts (Shen et al., 2011). (3) Laminar algal dolostone and bird's eyes structure in the lower Shuiquan Formation of MK section indicate the deposition in the intertidal-supratidal environments (Fig. S4). (4) The paleoflow direction reconstruction from the underlying Zhamoketi Formation also indicate the flow direct from southwest to northeast (Li and Dong, 1991).

2. Analytical Methods

2.1 Major and minor elemental composition analyses

Carbonate samples were crushed to 200 mesh. 30 mg powder sample was loaded in a 15 ml centrifuge tube and was dissolved in 10 ml Acetate-ammonium acetate buffer solution ($HAc:NH_4Ac$=1:5) with pH precisely adjusted to 4.5. In order to completely dissolve calcareous materials (both Ca-carbonate and dolomite), the centrifuge tubes were placed in a shaking table with a water bath temperature of 50℃ for 48 hours. After centrifugation, supernatant was collected for the element composition analysis. Elemental compositions were measured at Peking University by a Spectro Blue Sop inductively coupled plasma optical emission spectrometer (ICP-OES). All analyses were calibrated by series of gravimetric standards with different concentrations (ranging from 0.1-10 ppm) that were run before and after every twenty sample measurements. The element concentrations were calculated with respect to carbonate mass, i.e. $CaCO_3$+$MgCO_3$=100%. The analytical precisions for major and minor elements (Mg, Ca, Fe, Mn, Al) is ±5%.

2.2 Carbonate carbon ($\delta^{13}C_{carb}$) and oxygen isotope ($\delta^{18}O$) analyses

Mirrored thin and polished thick sections were prepared. Under the guidance of petrographic observation of thin section, sample powders were micro-drilled from the mirrored thick section to avoid sampling the diagenetic altered materials and hydrothermal veins. Carbon and oxygen isotopes were measured at the Oxy-Anion Stable Isotope Consortium (OASIC) of Louisiana State University by a Gas Bench coupled with an Isoprime 100 isotope ratio mass spectrometry. About 0.2 mg of carbonate powder was loaded in a headspace vial, and dried at 70°C for 24 hours. Five drops of phosphoric acid were added to the vial, and carbonate was converted CO_2 after reaction at 72 °C. The isotope ratios were reported in delta-notation as per mil deviation relative to the V-PDB Standard. The analytical precisions for $\delta^{13}C_{carb}$ and $\delta^{18}O$ are ±0.08‰ and ±0.1‰, respectively.

2.3 Organic Carbon Isotopes ($\delta^{13}C_{org}$) analyses

Fresh carbonate chips were crushed to 200 mesh, and ~30 mg sample powder was leached by 30 ml 3N HCl to dissolve all calcareous contents. The solution was centrifuged for 10 minutes at 3000 rpm and washed by Deionized water 3 times until pH > 5. The insoluble residues were dried down at 60°C in an oven. Organic Carbon Isotopes ($\delta^{13}C_{org}$) values were analyzed by a Vario Microcube Elemental Analyzer coupled with an Isoprime 100 isotope ratio mass spectrometry at the Oxy-Anion Stable Isotope Consortium (OASIC) of Louisiana State University. The isotope ratios were calibrated by the standard Acetanilide-OASIC (-27.62 ± 0.02‰), and the analytical precision for $\delta^{13}C_{org}$ is ±0.1‰.

3. Diagenetic evaluation of $\delta^{13}C_{carb}$

To evaluate whether $\delta^{13}C_{carb}$ values have been diagenetically altered, three geochemical proxies have been traditionally applied, (1) the absolute values of $\delta^{18}O$, (2) the relationship between $\delta^{13}C_{carb}$ and $\delta^{18}O$, and (3) Mn/Sr ratios (Jacobsen and Kaufman, 1999; Kaufman and Knoll, 1995; Knauth and Kennedy, 2009). Carbonate samples with $\delta^{18}O > -10$ ‰, Mn/Sr ratio <10, and the absence of the positive correlation between $\delta^{13}C_{carb}$ and $\delta^{18}O$, are regarded as least altered, suggesting that although the absolute $\delta^{13}C_{carb}$ values might be altered but the stratigraphic trend was preserved (Kaufman and Knoll, 1995). However, carbonate depositions during the Shuram Excursion normally show a positive correlation between $\delta^{13}C_{carb}$ and $\delta^{18}O$ values, and the $\delta^{18}O$ values are normally <-10‰ (Cui et al., 2017; Derry, 2010; Grotzinger et al., 2011). In fact, the global occurrence of SE is commonly considered to record a prominent ocean oxidation event rather than local diagenesis (Fike et al., 2006; McFadden et al., 2008; Shields et al., 2019), and the primary seawater signal has been supported by various geochemical and geological evidence (Gong and Li, 2020; Husson et al., 2015). $\delta^{18}O$ values in both MK and HZ sections range from −5‰ to −15‰, and show positive correlations with $\delta^{13}C_{carb}$ values (Figs.2, S5, Tables S2 and S3). We suggest that $\delta^{13}C_{carb}$ and $\delta^{18}O$ data cannot be applied to evaluate diagenetic alteration for SE samples. Negligible diagenetic alterations could be inferred from low Mn/Sr values (<3) of most MK samples (Fig. S5). On the other hand, it is noticed that although $\delta^{18}O$ values do not shift positively in the recovery of SE, the positive $\delta^{13}C_{carb}$ excursion is unlikely driven by a diagenetic alteration. In fact, similar pattern is observed in SE in Siberia as well (Melezhik et al., 2009; Pokrovskii et al., 2006) .

4. The global correlations of Shuram Excursions

There are three negative $\delta^{13}C_{carb}$ excursions in the Ediacaran period, in the chronological order, EN 1 in the cap carbonate immediately above the Marinoan glacial deposits at ~635 Ma, EN 2 represented by a brief negative $\delta^{13}C_{carb}$ excursion to ~-5‰ that might be correlated with the Gaskiers glaciation (~580 Ma), and EN 3 or the Shuram Excursion (SE) characterized by a long-duration negative $\delta^{13}C_{carb}$ excursion to as low as -12‰ between ~570 Ma and ~560 Ma (Gong and Li, 2020; McFadden et al., 2008). SE has been reported from Oman (Burns and Matter, 1993; Fike et al., 2006; Guerroue et al., 2006), Australia (Calver, 2000; Foden et al., 2001; Walter et al., 2000), the Unite States (Bergmann et al., 2011; Corsetti and J. Kaufman, 2003; Kaufman et al., 2007), India (Jiang et al., 2003; Kaufman et al., 2006), Scotland and Ireland (Prave et al., 2009), Siberia (Melezhik et al., 2009; Pokrovskii et al., 2006), Mongolia (Macdonald et al., 2009), South China (Jiang et al., 2007; McFadden et al., 2008; Tahata et al., 2013) and Tarim (Fig. S6). The most typical SE is recorded in the Nanfun Group in Oman, the Wonoka Formation in South Australia, the Doushantuo Formation in South China, the Johnnie Formation in the United State, and the Chencha Formation in Siberia (Grotzinger et al., 2011).

The characteristic features of SE include:

(1) **Magnitude and stratigraphic thickness.** Low $\delta^{13}C_{carb}$ values of ~-10‰ lasting for 10s to 100s m in stratigraphy (e.g., ~1000 m in Siberia, ~400 m in Oman, ~600 m in the United States, ~150 m in South Australia and ~50 m in South China) (Fig. S6).

(2) **Lithology, mainly in the shallow marine carbonate successions.** In Oman, SE initiates at the limestone of Khufai Formation and continues into the alternating carbonate and siliciclastic deposition of the Shuram Formation. In the United States, SE is recorded in the intercalated carbonate and siliciclastic deposition of the Johnnie and Stirling formations. In Australia, SE occurs in the dolostone of Wonoka Formation. In South China and Siberia, SE is recorded in the limestone, dolostone, and alternated depositions of limestone and marlstone (ribbon rock).

(3) **Stratigraphic asymmetry**. SE is characterized by a rapid drop and gradual recovery in $\delta^{13}C_{carb}$ values. In fact, the most negative values are started from a marine transgressive system, which may be responsible for the asymmetric expression of the SE. In contrast, the SE in the

Doushantuo Formation is interpreted as a high-stand system track rather than a transgressive system track (McFadden et al., 2008) and therefore shows a more symmetrical shape (Fig. S6).

(4) **Other geochemical signals**. Including the decoupling of carbonate carbon ($\delta^{13}C_{carb}$) and organic carbon ($\delta^{13}C_{org}$) isotopes (Swanson-Hysell et al., 2010), a strong positive correlation between $\delta^{18}O$ and $\delta^{13}C_{carb}$ (Derry, 2010), the concurrent decreasing of both $\delta^{34}S_{pyrite}$ and pyrite contents (Cui et al., 2015; Fike et al., 2006; McFadden et al., 2008), and the increases of $\delta^{238}U$ and $^{87}Sr/^{86}Sr$ (Cui et al., 2015).

5. Paleogeographic reconstruction of the absolute framework during the IITPW event from ca. 590-580 to 560 Ma

This absolute reconstruction is mainly after Robert et al. (2017, 2018) and Wen et al. (2020). The minimum-inertial moment axis (I_{min}) is indicated as the pole to the great circle by fitting the ca.590-560 Ma paleomagnetic poles (Fig. S7; Table S4). Key points for the reconstruction are provided in the following:

(1) ***West Gondwana.*** In this regime, except the Iapetus opening after 615 Ma (Cawood et al., 2001; Murphy et al., 2021), both geological (McGee et al., 2015; Tohver et al., 2010) and new paleomagnetic date (Wen et al., 2020) documented a wide (Clymene) ocean between Avalonia-Amazonia and West Africa (Figs. 3 and S7).

(2) ***Central Gondwana***. It is widely accepted that the northern part of the Central Gondwana had welded together at least by ca. 580 Ma (Schmitt et al., 2018), including the (620-580 Ma) Pan-African–Brasiliano collisional belt (Cordani et al., 2013; Ganade de Araujo et al., 2014) in its west and the (750-620 Ma) East African Orogen for the accretions of the Northeast Africa, India and Madagascar (Schmitt et al., 2018). The South China is linked to India after Yao et al. (2014), using the high-quality pole averaged from three regions of the upper most Doushantuo Formation (Jing et al., 2018). To the south, the Kalahari was not accreted to the south Congo Craton until early Cambrian (Meert, 2003; Robert et al., 2017).

(3) ***East Gondwana.*** The East Gondwana (including Australia and East Antarctic), together with the Kalahari Craton, accreted to the Central Gondwana through the 570-530 Ma Kuunga Orogeny (Meert, 2003).

(4) ***Two options for the Tarim Block.*** During the middle- to late-Ediacaran time, there is only one paleomagnetic pole from the 615 ± 6 Ma basaltic andesite of the uppermost Zhamoketi Formation (Zhao et al., 2014), field test is not available and only three quality factors (Q_f=7) of Van der Voo (1990) are satisfied (Table S4). So, two (T_1, T_2) optional positions are provided (Figs. 3 and S7). To the conventional view, Tarim is connected to northwestern Australia (T_1) at Rodinia's periphery during most Neoproterozoic time afterwards (ZX et al., 2008) and a little towards the Central Gondwana for its possible with India in the early Paleozoic (Zhao et al., 2018). Alternatively, Tarim was juxtaposed with North China in the position of T_2. The time patterns of accretionary-collisional events in Tarim are comparable to those in North China and

have been related to the assembly of East Gondwana during the early Paleozoic (Han et al., 2016). Recently, an integrated paleomagnetic and paleontological study suggested that North China played an important biogeographic link (Cambrian faunal exchange) between East Gondwana and Laurentia (Zhao et al., 2020). For its facilitation migrated from the conjugate margin of northwestern Laurentia in Rodinia's configuration (Ding et al., 2021; Zhao et al., 2019), North China is positioned somewhere between East Gondwana and Laurentia by adjusting the 514-505 Ma (Nc-XW and Nc-Hf) poles to the ca. 560 Ma group (Fig. S7). Then, the eastern Tarim (Quruqtagh and Chaidam) is adjacent to the western part of North China (current coordinates) because they both preserved the post-SE (≤560 Ma) glaciations (Zhou et al., 2019)(and this study) (Figs 1 and 3; Table S4). It is worth noting that this juxtaposition also can facilitate Tarim's migration from the "missing-link" connection, i.e., between Australia and Laurentia near the center of Rodinia (Ding et al., 2021; Wen et al., 2017; Wen et al., 2018) to this configuration through the middle to late Neoproterozoic. Additionally, the paleopole (T-Zma) from the Zhamoketi andesites is coincident with the ca. 560 Ma poles from other continents (Fig. S7) if a younger age is assigned, giving some quantitative constraints for this reconstruction.

6. Age constraints of Ediacaran glacial deposits in Figure 3

In the Figure 3, the Ediacaran glacial deposits in different continents (Fig.1, Table S1) are plotted in three paleogeographic maps, i.e., 590-580Ma, ~570Ma and ~560Ma maps. The assignments of glacial deposits are based on the available geochronology data (radiometric ages), chemostratigraphic data, biostratigraphic data (fossil records) and regional stratigraphic correlation. The paleogeographic distribution of glacial deposits should also accord with the non-Snowball Earth condition of the Ediacaran glaciation, i.e., the absence of low latitude glaciations.

Based on the quality of geochronology, chemostratigraphy, and biostratigraphy data, the ages of Ediacaran glacial deposits are variably constrained. For example, the Serra Azul Formation in Amazonia, the Gaskiers Formation in Avalonia, the Tiddiline Formation in West Africa and the Las Vantanas Formation in Rio Plata can be unambiguously identified as 590-580 Ma glaciations, while the Weesenstein/Clanzschwite/Orellana Formations in Cadomia, the Dhaiqa Formation in Arabia, the Kahar Formation in Iran, the Nudaus Formation in Kalahari, the Hankalchough Formation in Tarim and the Fersiga Formation in West Africa can be classified as ~560 Ma glaciations.

However, some Ediacaran glaciations can be placed into multiple paleogeographic maps based on the available age constraints. In this case, the glacial age can be additionally constrained by the principle of absence of low latitude glaciations in a non-Snowball Earth climatic condition (Fig.S8). For example, glacial deposits in Australia and Baltica are loosely constrained between 590 Ma from 560 Ma by geochronology data. Based on the new paleogeographic maps reconstructed in the context of IITPW event, South Australia and Baltica were placed in the tropical regions in both 580 Ma and 560 Ma maps (Figs. S8A and S8C), suggesting the presence of low latitude glaciations (e.g., the Egan Formation in northwestern Australia, the Billy Springs Formations in South Australia, the Groles Hill in Tasmania and the Moelv/Mortensnes Formation in Baltica), which is inconsistent with the non-Snowball Earth climatic condition. Thus, we can exclude these possible duration ranges (i.e., 590-580 Ma or ~560 Ma) and identify that the glacial deposits in both Australia and Baltica were deposited at ~570 Ma. In the same way, we can constrain the Abu Mahara Formation in Arabia, the Gwna Group, the Fauquier and Squantum Formations in Avalonia, the Loch na Cille Formation in

Laurentia at 590-580 Ma, and identify the Tanin-Starya Pechi glacial deposits in Siberia at ~570 Ma. The Hongtiegou Formation in Chaidam and Luoquan Formation in North China can be also classified as ~560 Ma glaciations, which are consistent with fossil records (Shen et al., 2007).

Finally, there are still some Ediacaran glacial depositions, whose ages remain loosely constrained even with the consideration of paleogeographic reconstruction, including the Santa Cruz Formation in Amazonia, the Nama Formation in Kalahari, the Iporanga Formation in Sao-Francisco, the Bokson diamictite in Siberia and the Ouarzazate Group in West Africa. These glacial deposits are marked as possible glaciations in all paleogeographic maps in Fig. 3.

References:

Bergmann, K.D., Zentmyer, R.A., Fischer, W.W., 2011. The stratigraphic expression of a large negative carbon isotope excursion from the Ediacaran Johnnie Formation, Death Valley. Precambrian Research 188, 45-56.

Burns, S.J., Matter, A., 1993. Carbon isotope record of the latest Proterozoic from Oman. Eclogae Geologicae Helvetiae 86, 595-607.

Calver, C.R., 2000. Isotope stratigraphy of the Ediacarian (Neoproterozoic III) of the Adelaide Rift Complex, Australia, and the overprint of water column stratification. Precambrian Research 100, 121-150.

Cawood, P.A., McCausland, P.J.A., Dunning, G.R., 2001. Opening Iapetus: Constraints from the Laurentian margin in Newfoundland. GSA Bulletin 113, 443-453.

Cordani, U.G., Pimentel, M.M., Ganade De Araújo, C.E., Basei, M.A.S., Fuck, R.A., Girardi, V.A.V., 2013. Was there an Ediacaran Clymene Ocean in central South America? American Journal of Science 313, 517.

Corsetti, F.A., J. Kaufman, A., 2003. Stratigraphic investigations of carbon isotope anomalies and Neoproterozoic ice ages in Death Valley, California. Geological Society of America Bulletin 115, 916-932.

Cui, H., Kaufman, A.J., Xiao, S., Zhou, C., Liu, X.-M., 2017. Methane-derived authigenic carbonates from the uppermost Doushantuo Formation in South China: Was the Ediacaran Shuram Excursion a globally synchronized early diagenetic event? Chemical Geology.

Cui, H., Kaufman, A.J., Xiao, S., Zhu, M., Zhou, C., Liu, X.-M., 2015. Redox architecture of an Ediacaran ocean margin: Integrated chemostratigraphic (δ13C–δ34S–87Sr/86Sr–Ce/Ce*) correlation of the Doushantuo Formation, South China. Chemical Geology 405, 48-62.

Derry, L.A., 2010. A burial diagenesis origin for the Ediacaran Shuram-Wonoka carbon isotope anomaly. Earth and Planetary Science Letters 294, 152-162.

Ding, J., Zhang, S., Evans, D.A.D., Yang, T., Li, H., Wu, H., Chen, J., 2021. North China craton: The conjugate margin for northwestern Laurentia in Rodinia. Geology.

Fike, D.A., Grotzinger, J.P., Pratt, L.M., Summons, R.E., 2006. Oxidation of the Ediacaran ocean. Nature 444, 744-747.

Foden, J., Barovich, K., Jane, M., O'Halloran, G., 2001. Sr-isotopic evidence for Late Neoproterozoic rifting in the Adelaide Geosyncline at 586 Ma: implications for a Cu ore forming fluid flux. Precambrian Research 106, 291-308.

Ganade de Araujo, C.E., Rubatto, D., Hermann, J., Cordani, U.G., Caby, R., Basei, M.A.S., 2014. Ediacaran 2,500-km-long synchronous deep continental subduction in the West Gondwana Orogen. Nature Communications 5, 5198.

Gao, Z., Zhu, S., 1984. Precambrian geology in Xinjiang, China. Xinjiang People's Publishing House, Urumuqi, China.

Gong, Z., Li, M., 2020. Astrochronology of the Ediacaran Shuram carbon isotope excursion, Oman. Earth and Planetary Science Letters 547, 116462.

Grotzinger, J.P., Fike, D.A., Fischer, W.W., 2011. Enigmatic origin of the largest-known carbon isotope excursion in Earth's history. Nature Geosci 4, 285-292.

Guerroue, E., Allen, P.A., Cozzi, A., Etienne, J.L., Fanning, M., 2006. 50-Myr recovery from the largest negative δ^{13}C excursion in the Ediacaran ocean. Terra Nova 18, 147-153.

Han, Y., Zhao, G., Cawood, P.A., Sun, M., Eizenhöfer, P.R., Hou, W., Zhang, X., Liu, Q., 2016. Tarim and North China cratons linked to northern Gondwana through switching accretionary tectonics and collisional orogenesis. Geology 44, 95-98.

Husson, J.M., Higgins, J.A., Maloof, A.C., Schoene, B., 2015. Ca and Mg isotope constraints on the origin of Earth's deepest C excursion. Geochimica et Cosmochimica Acta 160, 243-266.

Jacobsen, S.B., Kaufman, A.J., 1999. The Sr, C and O isotopic evolution of Neoproterozoic seawater. Chemical Geology 161, 37-57.

Jiang, G., Christie-Blick, N., Kaufman, A.J., Banerjee, D.M., Rai, V., 2003. Carbonate platform growth and cyclicity at a terminal Proterozoic passive margin, Infra Krol Formation and Krol Group, Lesser Himalaya, India. Sedimentology 50, 921-952.

Jiang, G., Kaufman, A.J., Christie-Blick, N., Zhang, S., Wu, H., 2007. Carbon isotope variability across the Ediacaran Yangtze platform in South China: Implications for a large surface-to-deep ocean δ13C gradient. Earth and Planetary Science Letters 261, 303-320.

Jing, X., Yang, Z., Tong, Y., Wang, H., Xu, Y., 2018. Identification of multiple magnetizations of the Ediacaran strata in South China. Geophysical Journal International 212, 54-75.

Kaufman, A.J., Corsetti, F.A., Varni, M.A., 2007. The effect of rising atmospheric oxygen on carbon and sulfur isotope anomalies in the Neoproterozoic Johnnie Formation, Death Valley, USA. Chemical Geology 237, 47-63.

Kaufman, A.J., Jiang, G., Christie-Blick, N., Banerjee, D.M., Rai, V., 2006. Stable isotope record of the terminal Neoproterozoic Krol platform in the Lesser Himalayas of northern India. Precambrian Research 147, 156-185.

Kaufman, A.J., Knoll, A.H., 1995. Neoproterozoic variations in the C-isotope composition of sea water: Stratigraphic and biogeochemical implications. Precambrian Research 73, 27-49.

Knauth, L.P., Kennedy, M.J., 2009. The late Precambrian greening of the Earth. Nature 460, 728-732.

Li, H., Dong, Y., 1991. Sedimentary features of the Sinian Zhamoketi Formation in the Middle Quruqtagh area of Xinjiang. Xinjiang Geology 9, 340-351.

Macdonald, F.A., Jones, D.S., Schrag, D.P., 2009. Stratigraphic and tectonic implications of a newly discovered glacial diamictite-cap carbonate couplet in southwestern Mongolia. Geology 37, 123-126.

McFadden, K.A., Huang, J., Chu, X., Jiang, G., Kaufman, A.J., Zhou, C., Yuan, X., Xiao, S., 2008. Pulsed oxidation and biological evolution in the Ediacaran Doushantuo Formation. Proceedings of the National Academy of Sciences 105, 3197-3202.

McGee, B., Collins, A.S., Trindade, R.I.F., Jourdan, F., 2015. Investigating mid-Ediacaran glaciation and final Gondwana amalgamation using coupled sedimentology and 40Ar/ 39Ar detrital muscovite provenance from the Paraguay Belt, Brazil. Sedimentology 62, 130-154.

Meert, J.G., 2003. A synopsis of events related to the assembly of eastern Gondwana. Tectonophysics 362, 1-40.

Melezhik, V.A., Pokrovsky, B.G., Fallick, A.E., Kuznetsov, A.B., Bujakaite, M.I., 2009. Constraints on 87Sr/86Sr of Late Ediacaran seawater: insight from Siberian high-Sr limestones. Journal of the Geological Society 166, 183-191.

Murphy, J.B., Nance, R.D., Cawood, P.A., Collins, W.J., Dan, W., Doucet, L.S., Heron, P.J., Li, Z.-X., Mitchell, R.N., Pisarevsky, S., Pufahl, P.K., Quesada, C., Spencer, C.J., Strachan, R.A., Wu, L., 2021.

Pannotia: in defence of its existence and geodynamic significance. Geological Society, London, Special Publications 503, 13.

Pokrovskii, B.G., Melezhik, V.A., Bujakaite, M.I., 2006. Carbon, oxygen, strontium, and sulfur isotopic compositions in late Precambrian rocks of the Patom Complex, central Siberia: Communication 1. results, isotope stratigraphy, and dating problems. Lithol Miner Resour 41, 450-474.

Prave, A.R., Fallick, A.E., Thomas, C.W., Graham, C.M., 2009. A composite C-isotope profile for the Neoproterozoic Dalradian Supergroup of Scotland and Ireland. Journal of the Geological Society 166, 845-857.

Robert, B., Besse, J., Blein, O., Greff-Lefftz, M., Baudin, T., Lopes, F., Meslouh, S., Belbadaoui, M., 2017. Constraints on the Ediacaran inertial interchange true polar wander hypothesis: A new paleomagnetic study in Morocco (West African Craton). Precambrian Research 295, 90-116.

Schmitt, R.d.S., Fragoso, R.d.A., Collins, A.S., 2018. Suturing Gondwana in the Cambrian: The Orogenic Events of the Final Amalgamation, in: Siegesmund, S., Basei, M.A.S., Oyhantçabal, P., Oriolo, S. (Eds.), Geology of Southwest Gondwana. Springer International Publishing, Cham, pp. 411-432.

Shen, B., Xiao, S., Bao, H., Kaufman, A.J., Zhou, C., Yuan, X., 2011. Carbon, sulfur, and oxygen isotope evidence for a strong depth gradient and oceanic oxidation after the Ediacaran Hankalchough glaciation. Geochimica et Cosmochimica Acta 75, 1357-1373.

Shen, B., Xiao, S., Dong, L., Zhou, C., Liu, J., 2007. Problematic macrofossils from Ediacaran successions in the North China and Chaidam blocks: implications for there evolutionary root and biostratigraphic significance. Journal of Paleontology 81, 1396-1411.

Shields, G.A., Mills, B.J.W., Zhu, M., Raub, T.D., Daines, S.J., Lenton, T.M., 2019. Unique Neoproterozoic carbon isotope excursions sustained by coupled evaporite dissolution and pyrite burial. Nature Geoscience 12, 823-827.

Swanson-Hysell, N.L., Rose, C.V., Calmet, C.C., Halverson, G.P., Hurtgen, M.T., Maloof, A.C., 2010. Cryogenian Glaciation and the Onset of Carbon-Isotope Decoupling. Science 328, 608-611.

Tahata, M., Ueno, Y., Ishikawa, T., Sawaki, Y., Murakami, K., Han, J., Shu, D., Li, Y., Guo, J., Yoshida, N., Komiya, T., 2013. Carbon and oxygen isotope chemostratigraphies of the Yangtze platform, South China: Decoding temperature and environmental changes through the Ediacaran. Gondwana Research 23, 333-353.

Tohver, E., Trindade, R.I.F., Solum, J.G., Hall, C.M., Riccomini, C., Nogueira, A.C., 2010. Closing the Clymene ocean and bending a Brasiliano belt: Evidence for the Cambrian formation of Gondwana, southeast Amazon craton. Geology 38, 267-270.

Walter, M.R., Veevers, J.J., Calver, C.R., Gorjan, P., Hill, A.C., 2000. Dating the 840–544 Ma Neoproterozoic interval by isotopes of strontium, carbon, and sulfur in seawater, and some interpretative models. Precambrian Research 100, 371-433.

Wen, B., Evans, D.A.D., Anderson, R.P., McCausland, P.J.A., 2020. Late Ediacaran paleogeography of Avalonia and the Cambrian assembly of West Gondwana. Earth and Planetary Science Letters 552, 116591.

Wen, B., Evans, D.A.D., Li, Y.-X., 2017. Neoproterozoic paleogeography of the Tarim Block: An extended or alternative “missing-link” model for Rodinia? Earth and Planetary Science Letters 458, 92-106.

Wen, B., Evans, D.A.D., Wang, C., Li, Y.-X., Jing, X., 2018. A positive test for the Greater Tarim

Block at the heart of Rodinia: Mega-dextral suturing of supercontinent assembly. Geology 46, 687-690.

Xiao, S., 2004. Neoproterozoic glaciations and biological evolution: Data from the Tarim and Yangtze blocks, China, in: Reimold, W.U., Hofmann, A. (Eds.), Abstract Volume of GSA/GSSA Field Forum "Processes on the Early Earth", p. 99.

Xu, B., Jian, P., Zheng, H., Zou, H., Zhang, L., Liu, D., 2005. U-Pb zircon geochronology and geochemistry of Neoproterozoic volcanic rocks in the Tarim Block of northwest China: implications for the breakup of Rodinia supercontinent and Neoproterozoic glaciations. Precambrian Research 136, 107-123.

Xu, B., Xiao, S., Zou, H., Chen, Y., Li, Z.-X., Song, B., Liu, D., Zhou, C., Yuan, X., 2009. SHRIMP zircon U–Pb age constraints on Neoproterozoic Quruqtagh diamictites in NW China. Precambrian Research 168, 247-258.

Zhao, G., Wang, Y., Huang, B., Dong, Y., Li, S., Zhang, G., Yu, S., 2018. Geological reconstructions of the East Asian blocks: From the breakup of Rodinia to the assembly of Pangea. Earth-Science Reviews 186, 262-286.

Zhao, H., Zhang, S., Ding, J., Chang, L., Ren, Q., Li, H., Yang, T., Wu, H., 2019. New geochronologic and paleomagnetic results from early Neoproterozoic mafic sills and late Mesoproterozoic to early Neoproterozoic successions in the eastern North China Craton, and implications for the reconstruction of Rodinia. GSA Bulletin 132, 739-766.

Zhao, H., Zhang, S., Zhu, M., Ding, J., Li, H., Yang, T., Wu, H., 2020. Paleomagnetic insights into the Cambrian biogeographic conundrum: Did the North China craton link Laurentia and East Gondwana? Geology 49, 372-376.

Zhao, P., Chen, Y., Zhan, S., Xu, B., Faure, M., 2014. The Apparent Polar Wander Path of the Tarim block (NW China) since the Neoproterozoic and its implications for a long-term Tarim–Australia connection. Precambrian Research 242, 39-57.

Zhou, C., Yuan, X., Xiao, S., Chen, Z., Hua, H., 2019. Ediacaran integrative stratigraphy and timescale of China. Sci. China Earth Sci. 62, 7-24.

ZX, L., SV, B., AS, C., A, D., B, D.W., 2008. Assembly, configuration, and break-up history of Rodinia: a synthesis. Precambrian Res. 160, 179.

Fig. S1.

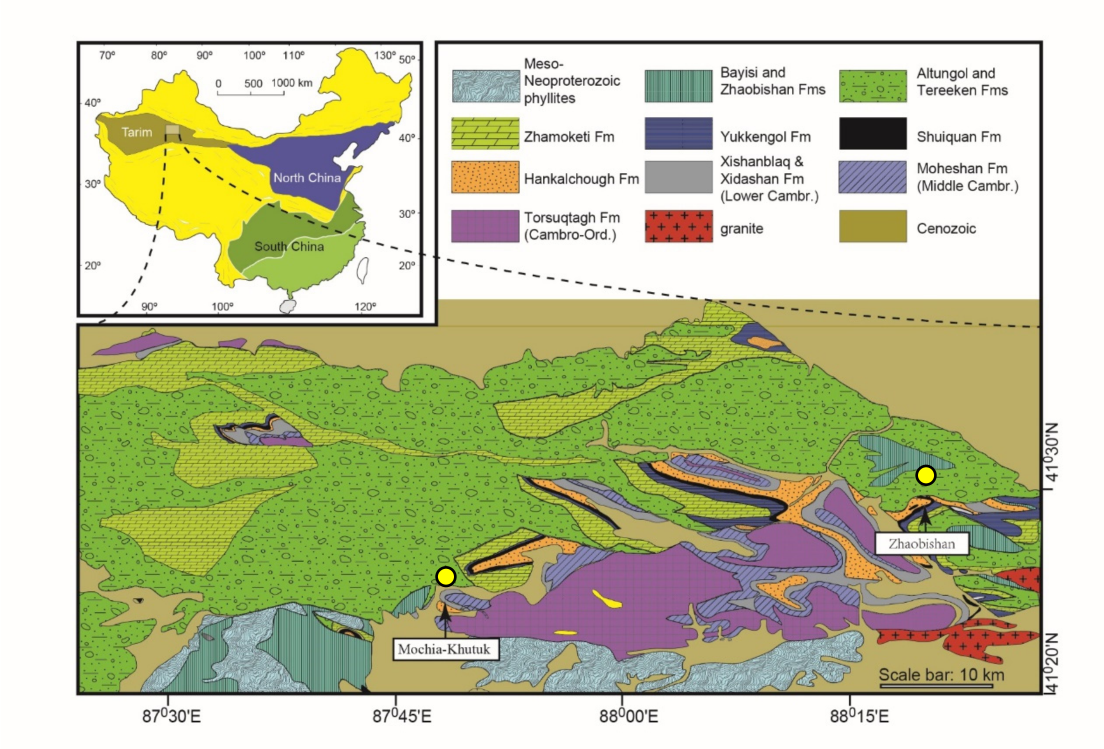

Figure S1: Geological map of the Quruqtagh area in the Tarim Block, northwestern China. The studied sections, Mochia-Khutuk (MK) and Heishan-Zhaobishan (HZ), are marked with yellow circles.

Fig. S2.

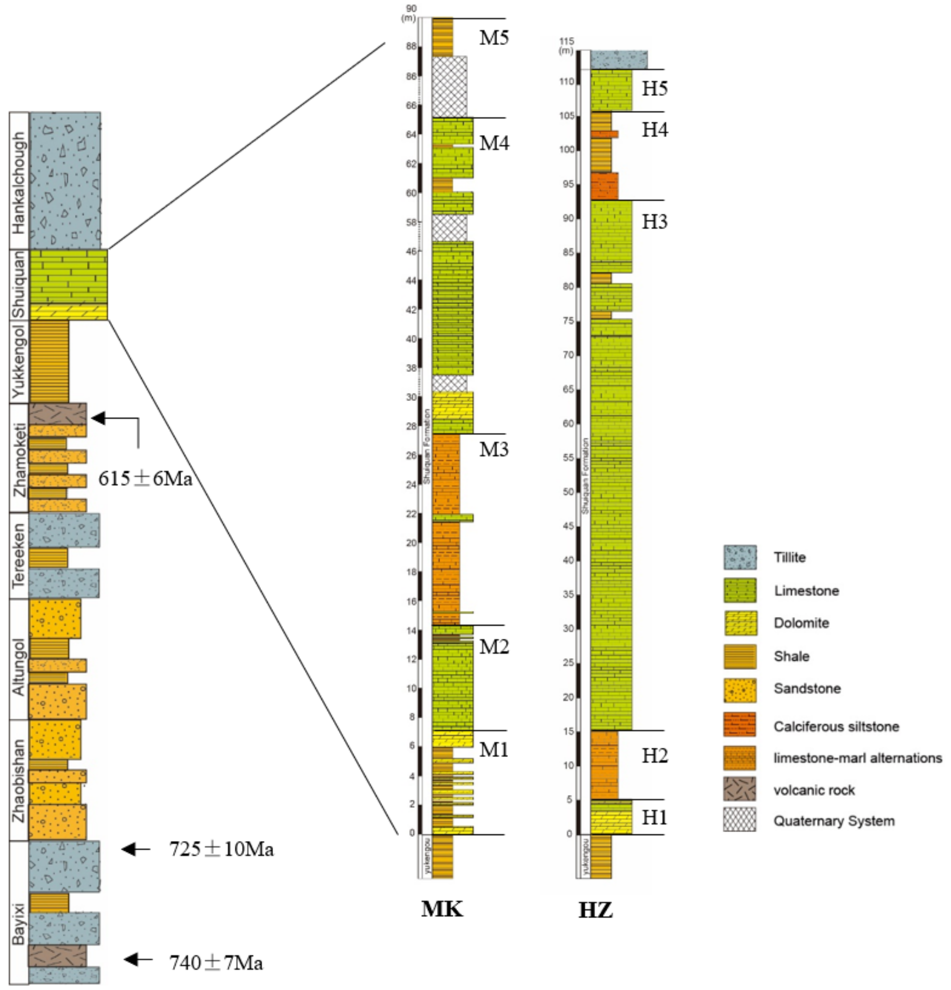

Figure S2: The lithostratigraphy of the Neoproterozoic Quruqtagh Group (left), and the lithostratigraphic column of the Shuiquan Formation in the Mochia-Khutuk (MK) and the Heishan-Zhaobishan (HZ) sections.

Fig. S3.

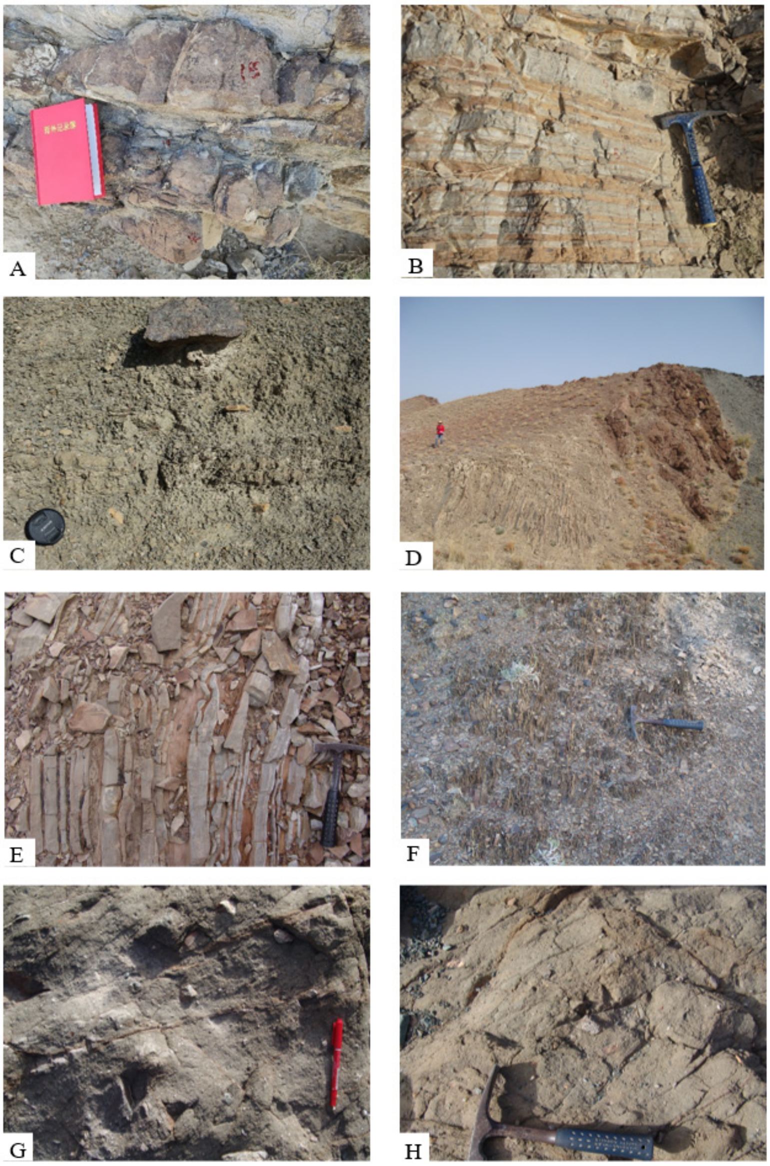

Figure S3: Field photographs of the Shuiquan and Hankalchough formations in the Quruqtagh area, Tarim Block. A: Reddish thin- to medium-bedded coarse crystalline dolostone (M2 in MK), B: Limestone-marl alternations (M3 in MK), C: Calcareous siltstone in the top of Shuiquan Formation (M5 in MK). D: The contact between the Shuiquan and Yukengou formation in HZ. The dolostone of the basal Shuiquan Formation overlies the dark gray siltstone/mudstone of the top of Yukengou Formation. E: Reddish-brown dolostone and light-gray limestone layers on the bottom of Shuiquan Formation (H1 in HZ). F: shale-calcareous siltstone in the top of Shuiquan Formation (H4 in HZ). G and H: Massive diamictite of the Hankalchough Formation (HZ).

Fig. S4.

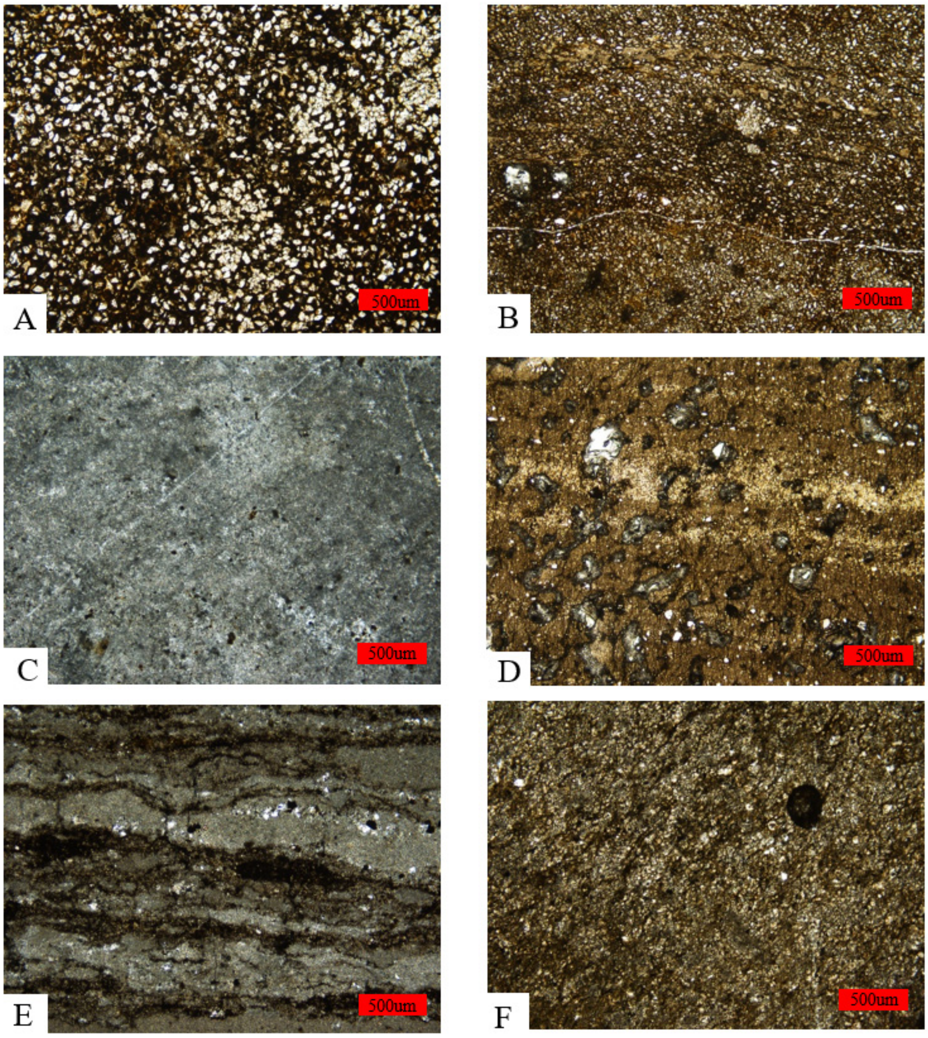

Figure S4: Photomicrographs of carbonate from the Shuiquan Formation.

Fig. S5.

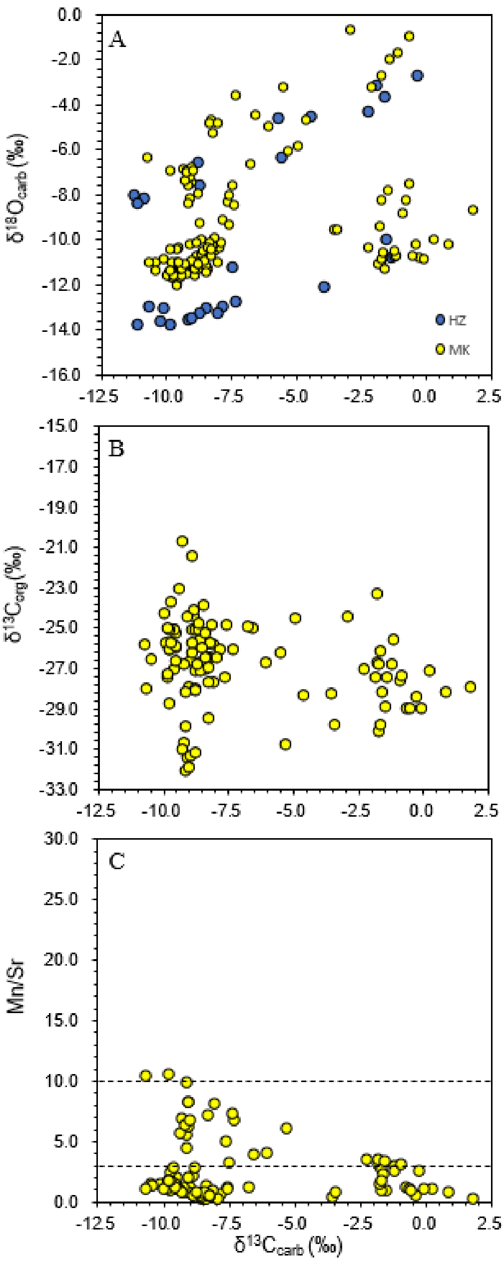

Figure S5: The element and isotope cross-plots. (a) $\delta^{13}C_{carb}$ vs. $\delta^{18}O$, (b) $\delta^{13}C_{carb}$ vs. $\delta^{13}C_{org}$, (c) $\delta^{13}C_{carb}$ vs. Mn/Sr ratios.

Fig. S6.

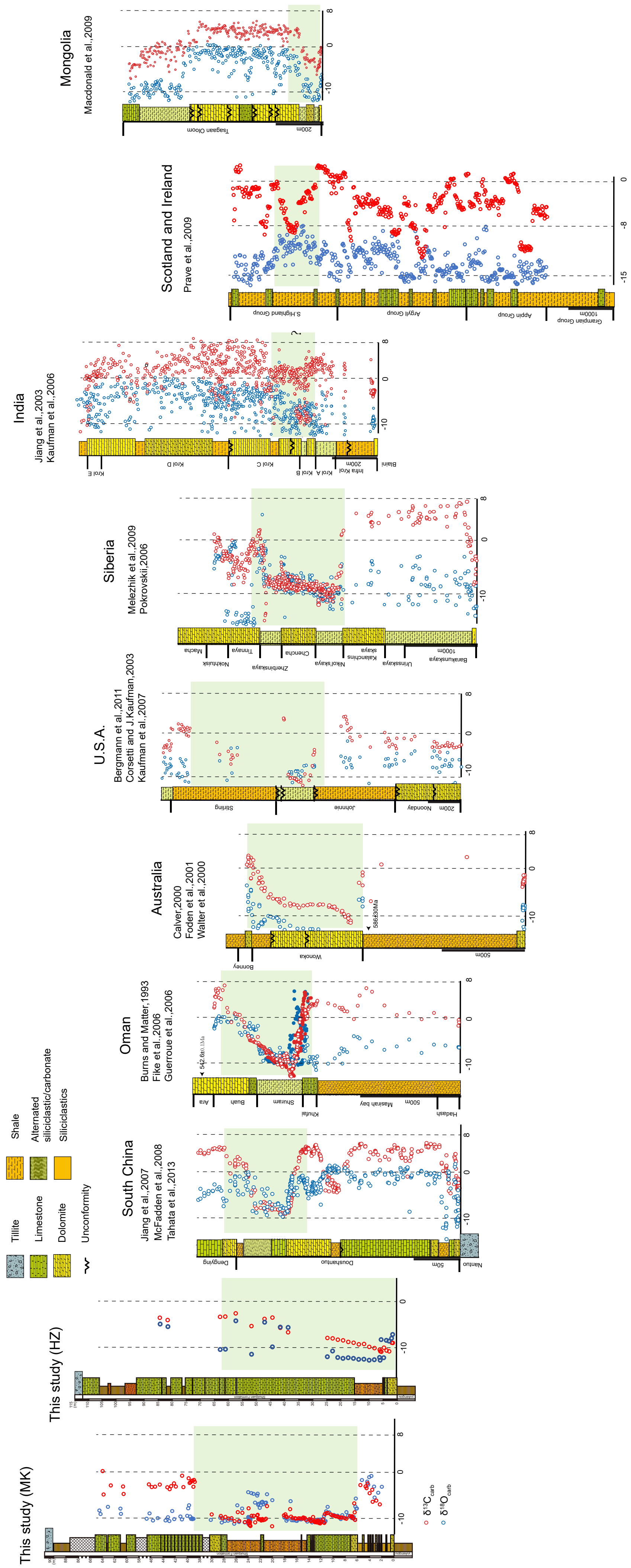

Figure S6: The global chemostratigraphic correlations of the Shuram excursion between different localities.

Fig. S7.

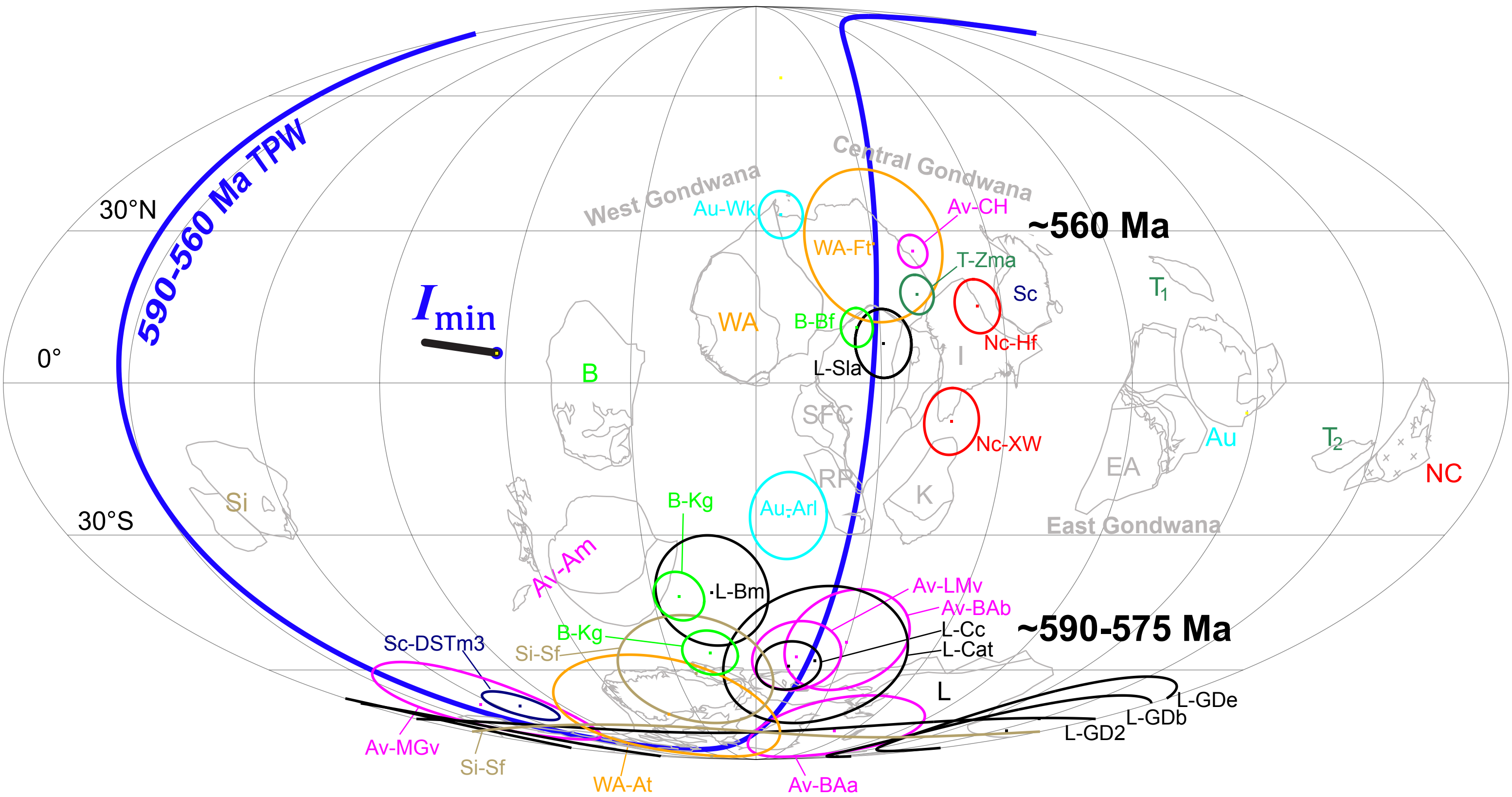

Figure S7: An absolute reconstruction at ca. 590-575 Ma (after Robert et al., 2017, 2018; Wen et al., 2020), showing the minimum inertial axis (I_{min}) as the pole to the great circle by fitting the 590-560 Ma paleomagnetic poles (Table S4) and two (T_1, T_2) possible positions for the Tarim Block. Reconstruction details are described in the Supplementary text. Relative rotation framework of different continents is shown in Fig. S9 and statistical parameters are summarized in Table S5. NC-North China, T-Tarim, CA-Chaidam, Au-Australia, EA- East Antarctica, WA-West Africa, NA-Northeast Africa, I-India, SC-South China, SFC-Sao Francisco-Congo, RP-Rio Plata, K-Kalahari, B-Baltica, Am-Amazonia, Av-Avalonia, Si- Siberia, L-Laurentia.

Fig. S8.

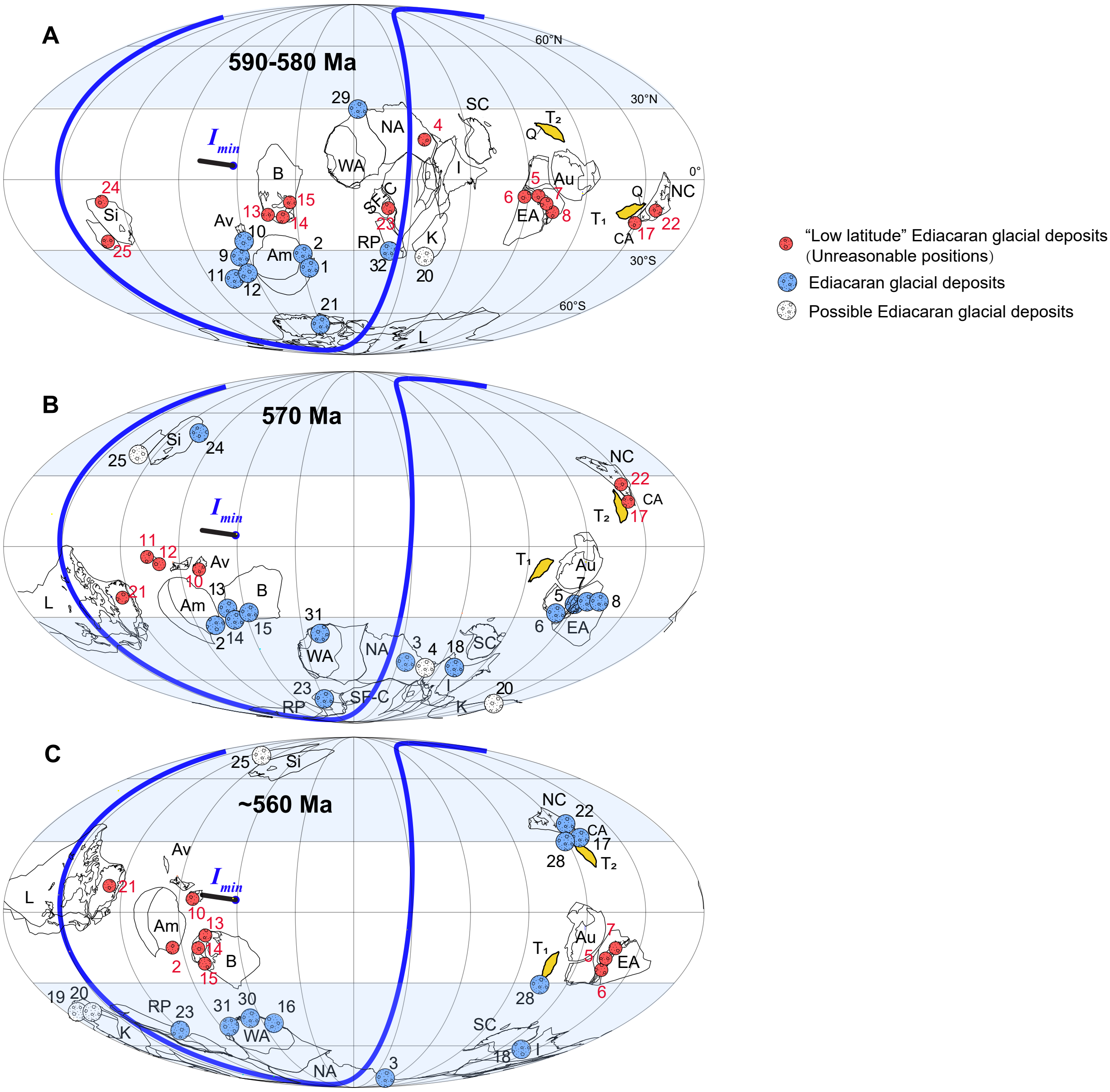

Figure S8: The possible geographic distributions of Ediacaran glacial deposits based on poor age constraints. Under a non-Snowball Earth climatic condition, the low-latitude Ediacaran glacial deposits is unlikely, marked as red circles. Meanwhile, the presence of low-latitude glaciations in these two intervals (A and C) argues against two separate non-Snowball Earth glaciations (i.e., ~580 Ma and ~560 Ma).

Fig. S9.

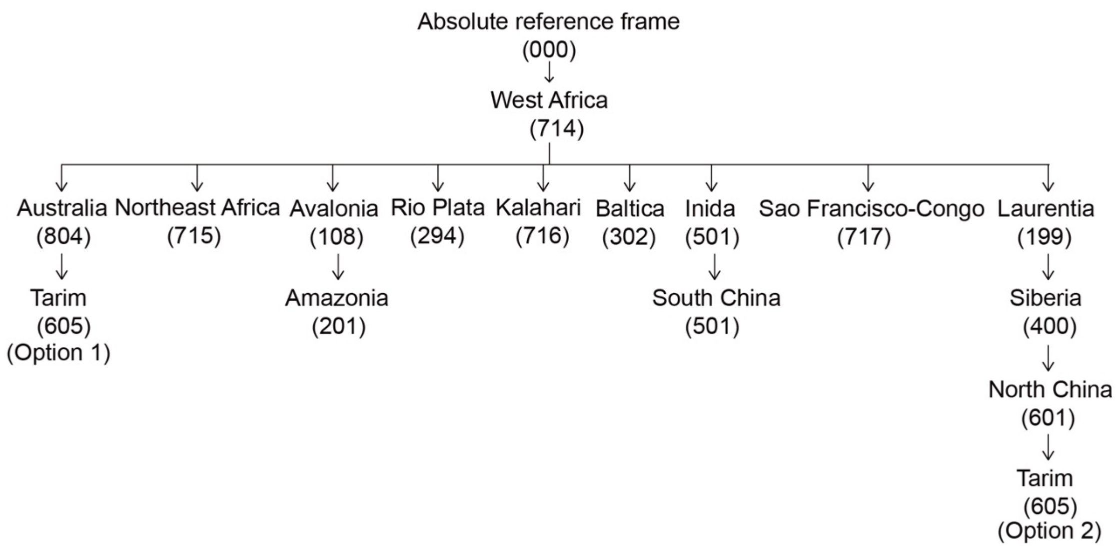

Figure S9: Relative rotation framework of different continents for the reconstructions in Figures 3 and S7. See rotation parameters in Table S5.

Table S1. Duration of Ediacaran glaciattion

No.	Palaeocontinent	Formation	Age	Succession/Basin	Country	Reference	Note
1	Amazonia	Serra Azul	630-580 Ma	Northern Paraguay belt	Brazil	(de Alvarenga et al., 2007; McGee et al., 2013, 2015)	Probably related to the Gaskiers Glaciation, with an age of approximately 580 Ma,U-Pb and Hf isotope data of detrital zircons from within this sequence
2		Santa Cruz	<587 Ma	Corumbá area	Certral Brazil	(Piacentini et al., 2013; Silva et al., 2016)	Minimum depositional age 587±7 Ma, $^{40}Ar/^{39}Ar$ geochronology
3	Arabia	Dhaiqa	<560 Ma		Saudi Arabia	(Vickers-Rich and Fedonkin, 2007)	An ash bed just below the diamictite provided a U –Pb age of 560±4 Ma .
4		Abu Mahara	620 Ma-570 Ma?		Oman	(Bowring et al., 2007)	Marinoan? Ediacaran? Not sure. U-Pb detrital zircon 620Ma; Estimated base of SE
5	Australia	Egan	<580 Ma ?	Kimberley region	Northwestern Australia	(Corkeron and George, 2001; Corkeron, 2007; 2008; 2011)	"Cap carbonates" correlation not similar with Marinoan, post-marinoan.
6		Billy Springs	620-550 Ma		South Australia	(Jenkins, 2011; Counts and Amos., 2016)	Wilpena Group (~620 Ma-550 Ma)
7		Croles Hill	<582 Ma	Kanunnah	Tasmania	(Calver et al., 2004)	U-Pb zircon, <582±4 Ma
8		Cottons Breccia	>575 Ma	Grassy Group	King Island	(Walter et al., 2000; Calver et al., 2004; Direen and Jago, 2008; Corkeron, 2011)	U-Pb zircon, >575±3 Ma ; stratigraphic correlation with Tasmania
9	Avalonia	Gaskiers	~580 Ma	Newfoundland	Canada	(Pu et al., 2016)	Tuff beds, between 580.90 ± 0.40 and 579.88 ± 0.44 Ma
10		Gwna Group	595-550 Ma	Anglesey Island, Wales	UK,Scotland	(Beckinsale et al., 1979; Kawai et al., 2008)	Holland Arms gneisses have a Rb–Sr whole rock isochron age of 595 ±12 Ma
11		Fauquier	582-571 Ma		USA	(Bowring et al., 2003; Southworth et al., 2009; Hebert et al., 2010)	U-Pb zircon, 582±0.4 Ma; U-Pb Zircon, 571±1 Ma
12		Squantum	595-570 Ma	Boston Basin	USA	(Sayles, 1914; Thompson and Bowring, 2000; Carto, 2012)	U-Pb tuff clast from Squantum diamictite; 595.5± 2 Ma. U-Pb ash bed; ~570 Ma

13	Baltica	Mortensnes	post-Marinoan	Verstertana	North Norway	(Edwards, 1984; Farmer et al., 1992; Chumakov, 2007; Rice et al., 2011)	No robust isotopic age constraints are available for the succession. $\delta^{13}C$ data, together with cap dolostone characteristics, offer paradigmic correlations with other areas (Smalfjord =Marinoan; Mortensnes= Gaskiers). A limited Ediacaran fauna, including Aspidella, give only broad age
14		Moelv	620~560 Ma	Sparagmite	South Norway	(Nystuen, 1976; Hannah et al., 2014; Bingen et al., 2005)	U-Pb and Lu-Hf detrital zircons; correlation
15		Vil'chitsy	>555 Ma	Eastern Europe		(Chumakov, 2004)	U-Pb zircon Xolyn Gabbro and Ust'Pinega?
16	Cadomia	Weesenstein/Clanzschwite/Orellana	560-540 Ma		West Africa	(Linnemann et al., 2018)	Zircons U-Pb age and Hf isotope analyses
17	Chaidam	Hongtiegou	~560 Ma?		China	(Shen et al., 2010; Pang et al., 2021)	Fossils (>547 Ma?)
18	Irania	Kahar Fm	<560 Ma	Alborz Mountains	Northern Iran	(Etemad-Saeed et al., 2016)	U–Pb detrital zircons(<563.1±3.9 Ma); chemostratigraphy
19	Kalahari	Nudaus Fm	549-545 Ma		Namibia	(Grotzinger et al., 1995; Germs and Gaucher, 2012; Hofmann et al., 2015)	U-Pb zircon age; Vingerbreek glaciation(post-Gaskiers 549-545 Ma); Vingerbreak Unconformity
20		Nama diamictite	~560 Ma?	Nama foreland basin	Namibila, South Africa	(Germs, 1995; Grotzinger et al., 1995)	635-530Ma, Fossils,Vingerbreak Unconformity
21	Laurentia	Loch na Cille	<601 Ma	Dalradian	British-Irish	(McCay et al., 2006; Chumakov, 2007)	~580Ma; U-Pb volcanics
22	North China	Luoquan	~560 Ma?	Qinling	China	(Guan et al., 1986; Heron et al., 2018)	Fossils
23	Sao-Francisco	Iporanga Fm	<580 Ma	São Francisco	Southeast Brazil	(Campanha et al., 2008)	U-Pb zircon SHRIMP ~580Ma is assigned for the base of this units
24	Siberia	Tanin-Starye Pechi	598-570 Ma	North and Middle Urals	Ural	(Chumakov, 2011; Maslov et al., 2013)	U-Pb zircons SHRIMP, volcanic tuffs, between 598±6 Ma and 567.2±3.9 Ma
25		Bokson diamictite	?		Mongolia	(Osokin and Tyzhinov, 1998; Kuzmichev, 2004; Chumakov,	Ediacaran? Cryogenian?
26		Zabit Fm	>560 Ma	East Sayan Mountains,Bokson Group	Weatern Buryatiya republic,Russia	(Chumakov et al., 2011)	Fossils: the Upper Vendian *Cloudian* sp. have been found in the diamictite matrix
27		Baykonur Formation	>560 Ma	Ulutau Mountains of central Kazakhatan	Kazakhstan/Kyrgyzstan, Asia	(Chumakov et al., 2009)	Fossils

28	Tarim	Hankalchough	<562 Ma	Quruqtagh	China	(Xiao et al., 2004; Xu et al., 2009)	this study, younger than SE
29	West Africa	Tiddiline	592-579 Ma	Anti-Atlas	Morocco	(Letsch et al., 2018; J.D.Inglis et al., 2005)	U-Pb zircon, between 592.31 ± 0.18 Ma and 579.4 ± 1.2 Ma; Anti-Atlas glaciation
30		Fersiga Group	556-519 Ma	Pourpree de l'Ahnet,Northwest Ahaggar	Algeria	(Bertrand-Sarfati et al., 1995)	Early Cambrian glaciation; 519±11 Ma (Rb/Sr isochron on whole rocks); 556+-12 Ma (U/Pb on zircon)
31		Ouarzazate Group	<~570 Ma	Anti-Atlas	Morocco	(Vernhet et al., 2012; Karaoui et al., 2015)	Bou-Azzer glaciations, Zircon U-Pb
32	Rio Plata	Las Vantanas	615-579 Ma	Western Gondwana	Uruguay	(Gaucher et al., 2008, Oyhantcabal et al., 2006)	K-Ar Basalt (615±30 Ma); Ar-Ar post-collisional plutons(579±1.5 Ma)

Table S2

Formation	Samples	Lithology	Height (m)	Carb. Content (%)	Mg/Ca	Fe/carb (ppm)	Mn/carb (ppm)	Al/carb (ppm)	Fe/Mn	Al/Mg	Mn/Sr	$\delta^{13}C_{carb}$ (‰)	$\delta^{18}O_{carb}$ (‰)	$\delta^{13}C_{org}$ (‰)	△carb-org (‰)
Shuiquan	19XE-SQ-51	black calcareous siltstone	95.00	2.11	0.435	250647.33	1553.60	1.29	161.33	3.23	1.64				
Shuiquan	19XE-SQ-50	black calcareous siltstone	93.00	0.69	0.592	4173991.12	8505.81	0.26	490.72	19.24	3.27				
Shuiquan	19XE-SQ-49	black calcareous siltstone	91.00	0.91	0.411	3063087.48	6537.56	1.51	468.54	21.19	2.16				
Shuiquan	19XE-SQ-48	black calcareous siltstone	89.00	1.56	0.141	1237743.50	3134.32	1.92	394.90	26.01	1.15				
Shuiquan	19XE-SQ-47	interbedded lime mudstone	64.80	90.57	0.001	8221.82	448.44	914.87	18.33	4.57	0.35	1.82	-8.64	-27.94	29.76
Shuiquan	19XE-SQ-46	interbedded lime mudstone	64.60	95.68	0.001	9490.41	558.26	1221.62	17.00	5.28	0.47	-3.56	-9.49	-28.28	24.71
Shuiquan	19XE-SQ-45	interbedded lime mudstone	63.30	88.37	0.002	6859.93	1038.16	2537.74	6.61	6.39	1.03	-1.49	-7.81	-28.95	27.46
Shuiquan	19XE-SQ-44	interbedded lime mudstone	61.60		0.002	3386.28	716.18	2175.00	4.73	5.17	0.99				
Shuiquan	19XE-SQ-43	interbedded lime mudstone	61.10	74.65	0.002	5329.69	918.46	2949.60	5.80	7.49	1.00	-1.71	-8.22	-30.11	28.39
Shuiquan	19XE-SQ-42	interbedded lime mudstone	61.00	85.72	0.002	3596.71	630.52	1988.20	5.70	4.04	0.84	-3.45	-9.49	-29.79	26.35
Shuiquan	19XE-SQ-41	thin-bedded limestone	46.47	60.32	0.004	22985.67	2888.01	14094.68	7.96	15.14	3.06	-1.19	-10.67	-25.60	24.41
Shuiquan	19XE-SQ-40	thin-bedded limestone	45.96	73.58	0.002	10060.67	2671.43	3639.05	3.77	7.68	3.10	-1.79	-9.40	-26.74	24.95
Shuiquan	19XE-SQ-39	thin-bedded limestone	45.37	77.12	0.002	9852.31	2529.56	3941.82	3.89	10.43	2.70	-1.71	-11.08	-26.83	25.11
Shuiquan	19XE-SQ-38	thin-bedded limestone	44.70	29.89										-27.23	
Shuiquan	19XE-SQ-37	thin-bedded limestone	44.52	72.45	0.002	8484.86	2305.02	3410.34	3.68	7.34	2.67	-1.20	-10.51	-26.81	25.61
Shuiquan	19XE-SQ-36	thin-bedded limestone	44.30	35.65											
Shuiquan	19XE-SQ-35	thin-bedded limestone	43.50	11.40										-28.23	
Shuiquan	19XE-SQ-34	thin-bedded limestone	43.16	57.58	0.002	13282.11	3132.72	5299.13	4.24	11.23	3.53	-1.84	-11.10	-27.46	25.62
Shuiquan	19XE-SQ-33	thin-bedded limestone	42.90	6.42										-27.17	
Shuiquan	19XE-SQ-32	thin-bedded limestone	42.73	74.15	0.001	6583.19	2826.13	3254.08	2.33	12.38	3.58	-2.26	-10.33	-27.08	24.81
Shuiquan	19XE-SQ-31	thin-bedded limestone	42.48	66.18	0.002	14911.90	2933.96	6461.48	5.08	11.98	3.46	-1.58	-11.24	-28.16	26.58
Shuiquan	19XE-SQ-30	thin-bedded limestone	41.97	47.27	0.005	28968.79	2938.54	16265.15	9.86	14.88	3.16	-0.92	-8.85	-27.66	26.74
Shuiquan	19XE-SQ-29	thin-bedded limestone	41.80	9.84										-27.68	
Shuiquan	19XE-SQ-28	thin-bedded limestone	41.63	60.18	0.002	11197.10	2173.44	5020.54	5.15	11.51	2.30	-1.67	-10.76	-26.12	24.46
Shuiquan	19XE-SQ-27	thin-bedded limestone	41.20												
Shuiquan	19XE-SQ-26	thin-bedded limestone	40.70	14.23										-25.55	
Shuiquan	19XE-SQ-25	marlstone and limestone	40.52	95.18	0.002	1874.84	657.88	356.24	2.85	0.63	0.88	0.86	-10.15	-28.15	29.00
Shuiquan	19XE-SQ-24	marlstone and limestone	40.27		0.002	5805.92	816.84	360.89	7.11	0.93	1.49	-1.76	-10.87		
Shuiquan	19XE-SQ-23	marlstone and limestone	39.33	95.17	0.002	3564.28	719.15	398.36	4.96	0.85	1.11	0.26	-10.01	-27.18	27.44
Shuiquan	19XE-SQ-22	marlstone and limestone	39.16	95.15	0.002	3025.54	859.71	219.72	3.52	0.57	1.28	-0.80	-8.22	-27.33	26.53
Shuiquan	19XE-SQ-21	marlstone and limestone	38.99	89.51	0.002	3938.91	714.44	311.38	5.51	0.75	1.06	-0.64	-7.48	-28.99	28.35
Shuiquan	19XE-SQ-20	marlstone and limestone	38.82		0.002	1922.35	666.33	258.09	2.88	0.51	0.63	-0.38	-10.15		
Shuiquan	19XE-SQ-19	marlstone and limestone	38.65	91.53	0.002	3130.10	2556.31	130.57	1.22	0.25	2.57	-0.27	-10.76	-28.43	28.17
Shuiquan	19XE-SQ-18-2	marlstone and limestone	38.50	68.73										-28.50	
Shuiquan	19XE-SQ-18-1	marlstone and limestone	38.48	73.73	0.001	2863.20	1444.36	669.19	1.98	2.44	1.70	-1.68	-10.58	-29.81	28.13

Shuiquan	19XE-SQ-17	marlstone and limestone	38.40	79.11	0.002	2523.62	893.47	381.57	2.82	0.75	1.15	-0.09	-10.82	-29.01	28.92
Shuiquan	19XE-SQ-16-2	marlstone and limestone	38.23	83.00	0.002	3882.99	760.56	804.81	5.11	1.98	0.91	-0.54	-10.72	-29.01	28.46
Shuiquan	19XE-SQ-16-1	marlstone and limestone	37.50	81.14										-27.46	
Shuiquan	19XE-SQ-15	marlstone and limestone	37.00	11.20										-29.54	
Shuiquan	19XE-SQ-14	marlstone and limestone	30.18	92.09	0.001	883.48	174.28	227.77	5.07	0.79	0.45	-8.04	-11.00	-27.69	19.65
Shuiquan	19XE-SQ-13	marlstone and limestone	29.90	88.43	0.001	1195.74	130.21	320.77	9.18	0.92	0.26			-25.84	
Shuiquan	19XE-SQ-12	marlstone and limestone	28.52	88.66	0.001	1311.42	503.54	235.17	2.60	0.83	1.42	-8.40	-10.49	-27.09	18.70
Shuiquan	19XE-SQ-11	marlstone and limestone	28.24	86.34	0.001	1434.64	320.52	235.57	4.48	0.94	0.72	-8.90	-11.62	-25.07	16.16
Shuiquan	19XE-SQ-10	marlstone and limestone	28.00												
Shuiquan	19XE-SQ-9	limestone-marl alternations	27.69	91.84	0.001	1664.60	343.87	268.59	4.84	1.07	0.74	-8.58	-11.27	-26.71	18.13
Shuiquan	19XE-SQ-8	limestone-marl alternations	27.14	89.50	0.001	1412.76	404.57	386.77	3.49	1.78	1.21	-8.97	-11.19	-26.59	17.62
Shuiquan	19XE-SQ-7	limestone-marl alternations	26.59	88.56	0.001	1686.80	741.77	220.62	2.27	1.07	2.16	-8.90	-10.97		
Shuiquan	19XE-SQ-6-1	limestone-marl alternations	26.04	80.84	0.001	1425.46	651.64	324.12	2.19	1.41	1.68			-23.58	
Shuiquan	19XE-SQ-6-2	limestone-marl alternations	25.80	84.49								-9.56	-11.94	-25.13	15.57
Shuiquan	19XE-SQ-5	limestone-marl alternations	25.48	71.78	0.037	18517.08	2014.97	564.72	9.19	0.07	3.26	-7.48	-7.55		
Shuiquan	19XE-SQ-4	limestone-marl alternations	25.21	94.38	0.001	1280.55	591.16	478.89	2.17	2.45	2.04	-9.51	-11.52		
Shuiquan	19XE-SQ-3	limestone-marl alternations	24.66	77.12	0.046	34657.84	4019.15	847.28	8.62	0.08	4.98	-7.63	-8.32	-27.46	19.83
Shuiquan	19XE-SQ-2	limestone-marl alternations	24.20	83.75	0.001	1831.76	889.20	449.05	2.06	1.35	2.45	-9.75	-11.63	-28.73	18.98
Shuiquan	19XE-SQ-1	limestone-marl alternations	24.00	62.89	0.001	1713.01	992.74	592.33	1.73	1.91	2.91	-9.59	-12.01	-27.02	17.43
Shuiquan	19MK-SQ2-1-1	limestone-marl alternations	23.55	72.25	0.031	17413.41	2195.48	584.65	7.93	0.08	3.87	-6.57	-4.44	-25.03	18.46
Shuiquan	19MK-SQ2-1-2	limestone-marl alternations	23.55	61.94	0.003	3940.31	618.73	1320.67	6.37	1.82	1.17	-9.51	-10.32	-25.27	15.75
Shuiquan	19MK-SQ2-2-1	limestone-marl alternations	23.40	64.06	0.001	2853.12	572.86	902.60	4.98	3.19	1.37	-9.60	-10.44	-25.93	16.33
Shuiquan	19MK-SQ2-2-2	limestone-marl alternations	23.40		0.001	2122.36	526.34	343.35	4.03	1.44	1.50	-10.09	-10.85		
Shuiquan	19MK-SQ2-3	limestone-marl alternations	23.37	66.66	0.001	2556.08	573.72	1157.20	4.46	5.21	1.58	-10.45	-11.02	-26.57	16.12
Shuiquan	19MK-SQ2-4-1	limestone-marl alternations	23.28	76.31	0.002	3281.19	801.73	1389.37	4.09	3.21	1.73	-9.82	-10.45	-27.46	17.65
Shuiquan	19MK-SQ2-4-2	limestone-marl alternations	23.28	79.64	0.001	2599.53	618.72	1434.62	4.20	6.61	1.41	-10.43	-11.33		
Shuiquan	19MK-SQ2-5	limestone-marl alternations	23.18	70.96	0.001	2366.80	534.11	752.53	4.43	3.21	1.13	-10.66	-11.00	-28.01	17.35
Shuiquan	19MK-SQ2-6	limestone-marl alternations	23.00	72.86	0.054	37410.61	3499.67	2566.92	10.69	0.21	7.22	-8.29	-4.64	-29.46	21.17
Shuiquan	19MK-SQ2-7-1	limestone-marl alternations	22.82	39.00	0.044	9620.66	3239.41	1203.21	2.97	0.12	6.78	-7.34	-3.57	-26.06	18.72
Shuiquan	19MK-SQ2-7-2	limestone-marl alternations	22.82	66.32								-8.31	-4.83	-25.73	17.42
Shuiquan	19MK-SQ2-8	limestone-marl alternations	22.63	74.75	0.060	34028.67	4329.09	4251.91	7.86	0.31	10.66	-9.83	-6.94	-27.30	17.47
Shuiquan	19MK-SQ2-9	limestone-marl alternations	22.36	40.05	0.050	37589.35	3794.45	1295.97	9.91	0.11	7.86			-26.30	
Shuiquan	19MK-SQ2-10	limestone-marl alternations	22.20	21.07										-25.74	
Shuiquan	19MK-SQ2-11	limestone-marl alternations	22.00	75.24								-8.22	-5.24	-26.46	18.24
Shuiquan	19MK-SQ2-12	limestone-marl alternations	21.99	79.47	0.054	17052.45	4042.11	232.05	4.22	0.02	8.13	-8.06	-4.79	-25.86	17.80
Shuiquan	19MK-SQ2-13	limestone-marl alternations	21.90	77.23	0.056	13740.94	3971.01	256.80	3.46	0.02	8.34	-9.03	-7.46	-27.91	18.88
Shuiquan	19MK-SQ2-14	limestone-marl alternations	21.80	77.93	0.065	34327.17	5746.83	318.24	5.97	0.02	5.66	-9.11	-7.19	-29.84	20.74
Shuiquan	19MK-SQ2-15	limestone-marl alternations	21.71	69.34	0.071	27615.23	5644.35	309.16	4.89	0.02	6.20	-9.06	-8.16	-31.40	22.34
Shuiquan	19MK-SQ2-16	limestone-marl alternations	21.53	79.75	0.073	30122.48	5255.23	2052.82	5.73	0.13	4.59			-29.24	

Shuiquan	19MK-SQ2-17	limestone-marl alternations	21.34	78.98	0.074	30270.22	5196.99	1801.23	5.82	0.11	4.57	-9.14	-7.56	-32.12	22.98
Shuiquan	19MK-SQ2-18	limestone-marl alternations	21.25	80.40	0.069	36343.36	5849.12	348.46	6.21	0.02	5.73	-9.37	-6.88		
Shuiquan	19MK-SQ2-19	limestone-marl alternations	21.16	78.97								-9.19	-6.91	-30.72	21.53
Shuiquan	19MK-SQ2-20	limestone-marl alternations	21.07	76.47	0.073	27844.40	5134.93	970.59	5.42	0.06	8.28	-9.02	-6.73	-31.93	22.91
Shuiquan	19MK-SQ2-21	limestone-marl alternations	20.88	84.08	0.077	33491.01	5354.93	990.48	6.25	0.06	6.92	-9.30	-7.33	-30.97	21.67
Shuiquan	19MK-SQ2-22	limestone-marl alternations	20.70	85.82										-31.73	
Shuiquan	19MK-SQ2-23	limestone-marl alternations	20.61	79.43	0.074	27948.59	4399.42	1337.45	6.35	0.08	6.34	-9.18	-6.98		
Shuiquan	19MK-SQ2-24	limestone-marl alternations	20.42	77.92	0.075	30094.44	5312.06	961.61	5.67	0.06	6.87	-8.96	-6.92	-31.37	22.40
Shuiquan	19MK-SQ2-25	limestone-marl alternations	20.24	92.84	0.083	7108.19	957.05	247.78	7.43	0.01	4.01	-6.06	-4.95	-26.74	20.68
Shuiquan	19MK-SQ2-26	limestone-marl alternations	19.32	92.21	0.082	17726.05	3669.59	192.11	4.83	0.01	10.44	-10.69	-6.37	-25.82	15.13
Shuiquan	19MK-SQ-72	limestone-marl alternations	17.20	89.25	0.001	1339.33	249.76	715.76	5.36	2.31	0.79	-8.16	-10.50	-24.82	16.66
Shuiquan	19MK-SQ-71	limestone-marl alternations	17.10	90.78										-25.63	
Shuiquan	19MK-SQ-70	limestone-marl alternations	16.93	91.98	0.001	1060.23	128.04	579.53	8.28	1.67	0.36	-7.94	-10.35		
Shuiquan	19MK-SQ-69	limestone-marl alternations	16.84	84.65	0.001	976.91	136.72	710.08	7.15	2.86	0.46	-8.41	-11.25	-25.85	17.44
Shuiquan	19MK-SQ-68	limestone-marl alternations	16.65	87.34	0.001	1178.51	120.55	683.83	9.78	2.26	0.37	-8.55	-10.87	-25.61	17.05
Shuiquan	19MK-SQ-67	limestone-marl alternations	16.10	81.54	0.036	9122.09	594.84	575.43	15.34	0.07	1.22	-6.73	-6.62	-24.94	18.22
Shuiquan	19MK-SQ-66	limestone-marl alternations	15.92	80.05	0.001	1019.14	123.19	655.16	8.27	2.51	0.27	-8.45	-11.14	-23.87	15.42
Shuiquan	19MK-SQ-65	limestone-marl alternations	15.64	84.46	0.001	1050.78	195.91	679.00	5.36	2.41	0.52	-8.77	-11.18	-25.06	16.29
Shuiquan	19MK-SQ-64	limestone-marl alternations	15.18	86.41	0.001	1079.30	208.90	396.91	5.17	1.29	0.59	-8.79	-11.25	-28.03	19.24
Shuiquan	19MK-SQ-63	limestone-marl alternations	15.00	82.62	0.001	1074.72	217.10	383.96	4.95	1.56	0.68	-8.93	-11.30	-26.23	17.30
Shuiquan	19MK-SQ-62	limestone-marl alternations	14.54	86.56	0.001	1223.13	191.43	484.51	6.39	1.64	0.60	-8.83	-10.91	-24.42	15.59
Shuiquan	19MK-SQ-61	limestone-marl alternations	14.26	87.60	0.001	1486.95	215.15	666.26	6.91	3.35	0.68	-8.87	-10.71	-21.46	12.59
Shuiquan	19MK-SQ-61A	limestone-marl alternations	13.80	73.58	0.001	1517.08	194.07	661.51	7.82	3.37	0.62	-8.86	-10.99	-24.06	15.19
Shuiquan	19MK-SQ-60	limestone-marl alternations	13.71	84.66	0.001	1453.37	185.19	503.24	7.85	2.44	0.44	-8.63	-10.62	-25.11	16.48
Shuiquan	19MK-SQ-59	limestone-marl alternations	13.43	83.36	0.001	1455.20	195.45	431.76	7.45	1.92	0.46	-8.77	-11.06	-27.17	18.40
Shuiquan	19MK-SQ-58	limestone-marl alternations	13.16	88.31	0.001	1411.32	218.78	337.14	6.45	1.39	0.85	-9.22	-11.47	-26.81	17.59
Shuiquan	19MK-SQ-57	limestone-marl alternations	13.00	86.02										-27.08	
Shuiquan	19MK-SQ-56	limestone-marl alternations	12.80	81.17										-25.30	
Shuiquan	19MK-SQ-55	limestone-marl alternations	12.60	88.42	0.001	1651.09	238.17	454.42	6.93	2.06	0.80	-9.01	-10.92		
Shuiquan	19MK-SQ-54	limestone-marl alternations	12.42	82.10	0.001	1730.81	322.39	366.96	5.37	1.51	1.31	-9.27	-11.13		
Shuiquan	19MK-SQ-53	limestone-marl alternations	12.33	87.53	0.001	1550.11	309.08	387.53	5.02	1.62	1.16	-9.48	-11.69	-26.58	17.10
Shuiquan	19MK-SQ-52	limestone-marl alternations	11.96	59.91	0.002	3426.07	312.99	1383.22	10.95	3.01	0.70	-8.49	-11.45		
Shuiquan	19MK-SQ-51-2	limestone-marl alternations	11.68									-9.58	-11.36		
Shuiquan	19MK-SQ-51-1	limestone-marl alternations	11.68	82.24	0.004	9092.55	505.14	523.29	18.00	0.58	1.16	-9.41	-11.61		
Shuiquan	19MK-SQ-50	limestone-marl alternations	11.59	71.04	0.001	1859.45	309.91	409.37	6.00	1.57	1.05	-9.70	-11.51	-23.69	13.99
Shuiquan	19MK-SQ-49	microcrystalline limestone	11.41	75.60	0.001	1952.00	342.68	534.65	5.70	1.97	1.07	-9.49	-11.31	-25.97	16.48
Shuiquan	19MK-SQ-48	microcrystalline limestone	11.32	80.77	0.001	1406.41	343.07	301.37	4.10	1.43	1.51	-9.57	-11.03	-25.13	15.56
Shuiquan	19MK-SQ-47	microcrystalline limestone	11.22	76.80	0.001	1509.44	377.36	278.06	4.00	1.26	1.50	-9.77	-11.42	-25.08	15.30
Shuiquan	19MK-SQ-46	microcrystalline limestone	11.13	69.13	0.001	1924.96	339.28	671.50	5.67	2.96	1.02	-9.38	-11.25	-23.05	13.68

Shuiquan	19MK-SQ-45	microcrystalline limestone	11.04	61.68	0.001	1996.73	288.97	595.33	6.91	2.20	0.77	-9.30	-11.04	-20.68	11.38
Shuiquan	19MK-SQ-44	microcrystalline limestone	10.95	81.19	0.001	1872.43	325.06	935.26	5.76	3.81	0.98	-9.77	-11.67	-26.05	16.27
Shuiquan	19MK-SQ-43	microcrystalline limestone	10.86	76.78	0.001	2020.47	341.26	1170.03	5.92	4.16	1.08	-9.90	-11.46	-25.76	15.86
Shuiquan	19MK-SQ-42	microcrystalline limestone	10.76	85.10	0.001	2096.62	395.48	955.90	5.30	4.16	1.69	-9.78	-10.99	-26.08	16.30
Shuiquan	19MK-SQ-41	microcrystalline limestone	10.67	69.26	0.002	7067.84	382.33	1416.49	18.49	3.32	1.06	-9.96	-11.62	-24.25	14.29
Shuiquan	19MK-SQ-40	microcrystalline limestone	10.40	74.92	0.002	2838.42	459.65	1335.73	6.18	3.12	1.31	-9.51	-10.97	-25.93	16.41
Shuiquan	19MK-SQ-39	microcrystalline limestone	10.25	83.48										-25.03	
Shuiquan	19MK-SQ-38	microcrystalline limestone	10.21	68.61	0.004	8384.34	816.98	1127.34	10.26	1.20	2.05	-9.07	-10.19	-24.48	15.41
Shuiquan	19MK-SQ-37	microcrystalline limestone	10.03	71.74	0.001	2719.40	639.86	801.27	4.25	2.75	1.80	-9.73	-11.55	-25.74	16.01
Shuiquan	19MK-SQ-36	microcrystalline limestone	9.94	62.31	0.001	1456.96	435.75	712.17	3.34	3.23	1.72	-9.84	-11.37	-25.05	15.20
Shuiquan	19MK-SQ-35	microcrystalline limestone	9.84	90.82	0.001	1207.07	241.41	1096.34	5.00	3.10	0.73	-7.84	-9.06	-26.07	18.23
Shuiquan	19MK-SQ-34	microcrystalline limestone	9.57	92.67	0.001	1002.38	397.25	771.85	2.52	2.41	1.21	-7.57	-7.99	-24.84	17.26
Shuiquan	19MK-SQ-33	microcrystalline limestone	9.29	96.53	0.001	1215.53	378.45	744.07	3.21	2.13	1.05	-7.56	-9.31		
Shuiquan	10MK-SQ-32	microcrystalline limestone	9.00	92.88										-26.78	
Shuiquan	19MK-SQ-31	microcrystalline limestone	8.74	92.40	0.001	1207.51	137.10	921.01	8.81	2.70	0.35	-7.93	-10.12	-26.52	18.59
Shuiquan	19MK-SQ-30	microcrystalline limestone	8.60	91.53										-25.70	
Shuiquan	19MK-SQ-29	microcrystalline limestone	8.46	92.03	0.001	1201.14	298.89	561.46	4.02	1.72	0.92	-8.10	-9.94		
Shuiquan	19MK-SQ-28	microcrystalline limestone	8.20	91.04										-26.88	
Shuiquan	19MK-SQ-27	microcrystalline limestone	8.10	91.15	0.001	1239.27	181.42	675.46	6.83	2.33	0.51	-8.22	-10.22	-25.73	17.52
Shuiquan	19MK-SQ-26	microcrystalline limestone	7.82	92.95	0.002	971.63	113.30	532.16	8.58	1.46	0.31	-8.35	-10.11	-26.45	18.11
Shuiquan	19MK-SQ-25	microcrystalline limestone	7.54	92.79	0.001	1021.68	185.29	666.69	5.51	2.05	0.56	-8.40	-10.52	-26.49	18.08
Shuiquan	19MK-SQ-24	microcrystalline limestone	7.27	92.38	0.001	1895.57	197.16	435.38	9.61	1.89	0.41	-8.53	-10.92	-25.99	17.47
Shuiquan	19MK-SQ-23	microcrystalline limestone	6.99	91.64	0.001	1112.97	215.13	899.62	5.17	2.77	0.73	-8.63	-9.98	-24.72	16.09
Shuiquan	19MK-SQ-22	microcrystalline limestone	6.81	92.58	0.001	1126.64	207.05	1012.86	5.44	3.04	0.59	-8.58	-10.51	-27.17	18.60
Shuiquan	19MK-SQ-21	microcrystalline limestone	6.26	92.72	0.001	1155.49	210.88	993.41	5.48	2.93	0.73	-8.73	-9.28	-26.78	18.05
Shuiquan	19MK-SQ-20	microcrystalline limestone	5.98	92.28	0.001	1225.59	204.26	897.69	6.00	2.93	0.62	-8.87	-10.10	-25.73	16.86
Shuiquan	19MK-SQ-19	microcrystalline limestone	5.34	92.64	0.001	1266.62	211.96	741.85	5.98	2.51	0.63	-8.26	-10.67	-26.97	18.72
Shuiquan	19MK-SQ-18	microcrystalline limestone	5.06	93.09	0.001	1185.51	222.95	636.70	5.32	2.28	0.77	-8.41	-10.34	-25.29	16.88
Shuiquan	19MK-SQ-17	microcrystalline limestone	4.97	93.28	0.001	1519.38	247.96	722.01	6.13	2.69	0.59	-8.26	-10.44	-27.75	19.48
Shuiquan	19MK-SQ-16	microcrystalline limestone	4.78	90.68	0.001	1326.26	313.96	625.90	4.22	2.00	0.76	-8.75	-11.06	-28.06	19.31
Shuiquan	19MK-SQ-15	limestone	4.69	91.43	0.077	21375.25	3422.17	304.42	6.25	0.02	2.83	-8.78	-7.95	-31.19	22.42
Shuiquan	19MK-SQ-14	limestone	4.60	82.75	0.082	12191.67	3172.75	186.08	3.84	0.01	6.13	-5.31	-6.03	-30.78	25.47
Shuiquan	19MK-SQ-13	limestone	4.51	54.02	0.079	30411.90	7441.18	507.94	4.09	0.03	7.29	-7.36	-8.45		
Shuiquan	19MK-SQ-12	limestone	4.42	87.22	0.084	36968.58	10291.88	360.93	3.59	0.02	9.93	-9.13	-8.39	-28.19	19.06
Shuiquan	19MK-SQ-11	limestone	3.50	36.30	0.068	44001.35	12396.36	19851.40	3.55	1.28	42.35	-1.08	-1.64		
Shuiquan	19MK-SQ-10	limestone	2.58	70.20	0.075	41126.60	16293.08	10241.51	2.52	0.60	41.63	-1.39	-2.02	-27.48	26.09
Shuiquan	19MK-SQ-9	limestone	2.39	83.00	0.079	51970.41	18354.04	6567.90	2.83	0.37	33.41	-1.76	-2.75	-23.31	21.55
Shuiquan	19MK-SQ-8	shale	2.30	72.66										-25.29	
Shuiquan	19MK-SQ-7	limestone	2.21	48.89	0.077	34346.26	16004.59	8760.90	2.15	0.51	35.73	-0.65	-0.96		

Shuiquan	19MK-SQ-6	limestone	1.84	62.47	0.060	12363.95	19329.70	5746.00	0.64	0.42	44.84	-2.92	-0.67	-24.42	21.50
Shuiquan	19MK-SQ-5	limestone	1.38	40.97	0.076	67851.51	22006.04	7102.36	3.08	0.42	38.98	-2.14	-3.22		
Shuiquan	19MK-SQ-5A	limestone	1.29	74.00	0.069	70155.56	29993.84	4019.62	2.34	0.26	47.85	-4.91	-5.82	-24.55	19.64
Shuiquan	19MK-SQ-4	shale	0.80												
Shuiquan	19MK-SQ-3	limestone	0.64	72.09	0.072	64297.94	36453.19	4979.15	1.76	0.31	36.82	-4.62	-4.68	-28.33	23.71
Shuiquan	19MK-SQ-2	shale	0.30	9.54										-27.71	
Shuiquan	19MK-SQ-1	limestone	0.00	67.36	0.071	25761.20	56680.31	4692.32	0.45	0.29	49.47	-5.50	-3.26	-26.26	20.76

Table S2: Carbonate Carbon ($\delta^{13}C_{carb}$) , Oxygen Isotopes($\delta^{18}O$) and Organic Carbon Isotopes ($\delta^{13}C_{org}$) of Shuiquan Formation, Mochia-Khutuk (MK) section, South China.

Table S3

Formation	Samples	Lithology	Height (m)	$\delta^{13}C_{carb}$ (‰)	$\delta^{18}O_{carb}$ (‰)
Shuiquan	AFQ536	shale-calcareous siltstone	434.5		
Shuiquan	AFQ537	shale-calcareous siltstone	436		
Shuiquan	AFQ538	shale-calcareous siltstone	438		
Shuiquan	AFQ539	shale-calcareous siltstone	439		
Shuiquan	AFQ540	shale	442		
Shuiquan	AFQ541	thin-bedded limestone	443		
Shuiquan	AFQ542	shale	448		
Shuiquan	AFQ543	shale-calcareous siltstone	452		
Shuiquan	AFQ544	thin-bedded limestone	458	-1.6	-3.6
Shuiquan	AFQ545	thin-bedded limestone	461	-2.2	-4.4
Shuiquan	AFQ546	thin-bedded limestone	471		
Shuiquan	AFQ547	thin-bedded limestone	476		
Shuiquan	AFQ548	thin-bedded limestone	481	-1.3	-10.7
Shuiquan	AFQ549	thin-bedded limestone	483	-1.2	-10.7
Shuiquan	AFQ550	thin-bedded limestone	487	-0.3	-2.7
Shuiquan	AFQ551	thin-bedded limestone	490		
Shuiquan	AFQ552	thick-bedded limestone	493	-3.9	-12.1
Shuiquan	AFQ553	thick-bedded limestone	498	-1.9	-3.1
Shuiquan	AFQ554	thick-bedded limestone	501	-1.5	-10.0
Shuiquan	AFQ555	thick-bedded limestone	504	-4.4	-4.5
Shuiquan	AFQ556	thick-bedded limestone	507	-5.7	-4.6
Shuiquan	AFQ557	light-gray limestone	522	-7.3	-12.8
Shuiquan	AFQ558	light-gray limestone	524	-7.4	-11.2
Shuiquan	AFQ559	light-gray limestone	526	-7.8	-13.0
Shuiquan	AFQ560	light-gray limestone	528	-8.0	-13.2
Shuiquan	AFQ561	light-gray limestone	530	-8.4	-13.0
Shuiquan	AFQ562	limestone-marl alternations	532	-8.7	-13.2
Shuiquan	AFQ563-a	brown limestone		-5.6	-6.4
Shuiquan	AFQ563-b	limestone-marl alternations	534	-9.1	-13.5
Shuiquan	AFQ564	limestone-marl alternations	536	-9.0	-13.5
Shuiquan	AFQ565	limestone-marl alternations	538	-9.9	-13.7
Shuiquan	AFQ566	limestone-marl alternations	540	-10.2	-13.6
Shuiquan	AFQ567	limestone-marl alternations	542	-10.7	-13.0
Shuiquan	AFQ568	limestone-marl alternations	542.2	-11.1	-13.7
Shuiquan	AFQ569	reddish-brown dolomite	542.6	-11.2	-8.0
Shuiquan	AFQ570	light-gray limestone	543.6	-10.1	-13.0
Shuiquan	AFQ571	reddish-brown dolomite	544.6	-10.9	-8.2
Shuiquan	AFQ572	reddish-brown dolomite	545.6	-11.1	-8.4
Shuiquan	AFQ573	reddish-brown dolomite	546.6	-8.7	-7.6
Shuiquan	AFQ574	reddish-brown dolomite	547	-8.7	-6.6

Table S3: Carbonate Carbon ($\delta^{13}C_{carb)}$, Oxygen Isotopes($\delta^{18}O$) and Organic Carbon Isotopes ($\delta^{13}C_{org}$) of Shuiquan Formation, Heishan-Zhaobishan (HZ) section, South China.

Table S4. Paleomagnetic poles for the abslute reconstruction in Figures 3 and S7

Pole ID	Rock Unit (Area)	Age (Ma)	Age range (Ma) Max	Min	P-lat (°N)	P-long (°E)	A_{95} (°)	1	2	3	4	5	6	7	Q_f	Reference
Laurentia (L)																
L-Sla	Sept-Iies intrusion (Shallow)	565 ± 4	569	561	-20	321	6.7	1	1	1	1	1	0	0	5	Tanczyk et al., 1987
L-Cat	Catoctin Basalts (steep)	572 ± 5	577	567	42	297	17.0	1	1	1	1	1	1	1	7	Meert et al., 1994
L-Cc	Callander Alkaline Complex intrusive	577 ± 1	578	576	46	301	6.0	1	1	1	1	0	1	1	6	Symons and Chiasson, 1991
L-Bm	Baie des Moutons complex	583 ± 2	585	581	42.6	332.7	12.0	1	1	1	0	0	0	1	4	McCausland et al., 2011
L-GDb	Grenville Dikes (Steep)	587.3 ± 0.7	588	587	55.7	233.4	10.6	1	1	1	1	1	0	1	6	Halls et al., 2015
L-GDe	Grenville Dikes (Steep)	586 ± 4	590	581	51.5	231.2	11.6	1	1	1	1	1	0	1	6	Hyodo and Dunlop, 1993
L-GD2	Grenville Dikes (Steep)	590 ± 2	592	588	61.6	249.9	14.5	1	1	0	1	1	1	1	6	Murthy, 1971
Avalonia (Av)																
Av-CH	Crown Hill Fm, Newfoundland, Canada	< 557+/-14 Ma; 566+/-13	570	540	-48.1	9.9	3.3	1	1	1	1	1	1	1	7	Wen et al., 2020
Av-BAb	Bonavista Bull Arm Fm, Newfoundland, Canada	592 ± 2.2; 591.3 ± 1.6	594	589	-15.5	278.2	11.9	1	1	1	1	1	1	1	7	Wen et al., 2020
Av-BAa	Argentia Bull Arm Formation, Newfoundland, Canada	< 600			-2.9	256.3	10.6	0	1	1	1	1	1	1	6	Pisarevsky et al., 2012; reference age of Mills et al., 2017
Av-MGv	Marystown Group volcanic-sedimentary sequence, Newfoundland, Canada	585 ± 2; 580 ± 3; 576.8 ± 2.6; 575 ± 2	587	573	26.6	239.6	11.1	1	1	1	1	1	1	1	7	McNamara et al., 2001; Sparkes and Dunning, 2014
Av-LMv	Lynn-Mattapan Volcanics, New England, USA	595.8 ± 1.2; 597.4 ± 1.5; 596.0 ± 1.4; 595.7 ± 1.6	599	594	60	206	8.4	1	1	1	1	1	1	1	7	Thompson et al., 2007
West Africa (WA)																
WA-Ft	Fajjoud and Tadoughast Volcanics, Morocco	566 ± 6; 564 ± 6; 567 ± 5; 565 ± 5; 556± 5	572	551	21.9	31	15.6	1	1	1	1	0	1	1	6	Robert et al., 2017, 2018
WA-At	Adrar-n-takoucht Volcanics	572 ± 5; 570 ± 6	577	564	-57.6	295.6	15.7	1	0	1	1	0	1	1	5	Robert et al., 2017, 2018
Australia (Au)																
Au-Wk	Wonoka Formation, S. Australia	~ 565	Fossils		-5.2	30.5	4.9	0	1	1	1	1	1	1	6	Schmidt and Williams, 2010
Au-Arl	Lower Arumbera sandstone	~ 570	Strati		-53.9	348.1	8.8	0	0	1	1	1	1	1	5	Mitchell et al., 2010

Baltica (B)															
B-Bf	Basu Formation	570-560	Fossils		-2	6	3.8	1	1	1	1	1	1	0	6	Levashova et al., 2015
B-Kg	Kurgashlya formation	600-570?			50.9	314.5	5.3	0	1	1	1	1	1	1	6	Lubnina et al., 2014
B-Bk	Bakeevo formation	600-570?			42.3	299.1	5.3	0	1	1	1	1	1	1	6	Lubnina et al., 2014
Tarim (T)																
T-Zma	Zhamoketi Formation	< 600			4.9	326.7	3.9	0	1	1	0	0	0	1	3	Zhao et al., 2014
Siberia (Si)																
Si-Mf	Minya Formation	590-570			33.7	217.2	12.7	0	0	1	0	1	1	0	3	Kravchinsky et al., 2001
Si-Sf	Shaman Formation	590-570	Fossils		32	251.1	13.8	0	1	1	1	1	1	0	5	Kravchinsky et al., 2001
South China (Sc)																
Sc-DSTm3	Doushantuo Formation Member3	591.1 ± 5.3	596	586	-31.3	349.8	4.1	0	1	1	1	1	1	1	6	Jing et al., 2018; age from Zhu et al., 2013
North China (Nc)																
Nc-Hf	Hsuchuang Formation	505	Fossils		31.8	320.4	5.3	1	1	1	1	1	1	0	6	Zhao et al., 2020
Nc-XW	Xinjin and Wudaotang formations	514-509	Fossils		18.5	341.9	6.5	1	1	1	1	1	0	1	6	Huang et al., 1999

Notes: P-lat/P-long, latitude/longitude of a paleomagnetic pole. A_{95}, radius of the pole 95% confidence cone. Q_f, Q-factor of Van der voo,1990.

Table S5. Rotation parameters for the absolute reconstruction in this study

Plate ID	Age	Euler Pole		Angle of rotation	Relative to
	Ma	(°N)	(°E)	(°)	
West Africa(714)	560	-5.8	111.8	105.7	Absolute reference(000)
West Africa(714)	590	-20.8	-169.7	-16.9	Absolute reference(000)
Northeast Africa(715)	590-560	-26.3	-164.4	0.5	West Africa(714)
Sao Francisco-Congo(717)	590-560	-68.4	-135.8	0.3	West Africa(714)
Kalahari(716)	590-560	-52.9	-76.5	-5.0	West Africa(714)
Rio Plata(294)	590-560	-73.9	134.2	-62.0	West Africa(714)
India(501)	590-560	41.4	24.2	302.6	West Africa(714)
South China(602)	590-560	23.4	92.7	78.2	India(501)
Baltica(302)	590-560	9.1	9.3	99.3	West Africa(714)
Avalonia(108)	590-560	-5.8	158.8	-84.1	West Africa(714)
Amazonia(201)	590-560	-12.9	36.7	327.1	Avalonia(108)
Laurentia(199)	590-560	-3.8	169.3	-137.9	West Africa(714)
Australia(804)	590-560	-21.6	-54.6	43.3	West Africa(714)
Siberia(400)	590-560	54.6	162.3	-302.6	Laurentia(199)
North China(601)	590-560	-17.9	-51.0	172.9	Siberia(400)
Tarim(605) option 1	590-560	12.1	95.7	197.3	Australia(804)
Tarim(605) option 2	590-560	14.9	109.8	332.5	North China(601)

References (Table S1):

Beckinsale, R.D., Thorpe, R.S., 1979. Rubidium–strontium whole-rock isochron evidence for the age of metamorphism and magmatism in the Mona Complex of Anglesey. Journal of the Geological Society, London 136, 433–439.

Bertrand-Sarfati, J., Moussine-Pouchkine, A., Amard, B., Ait Kaci Ahmed, A., 1995. First Ediacaran fauna found in western Africa and evidence for an Early Cambrian glaciation. Geology 23, 133-136.

Bingen, B., Griffin, W.L., Torsvik, T.H., Saeed, A., 2005. Timing of Late Neoproterozoic glaciation on Baltica constrained by detrital zircon geochronology in the Hedmark Group, south-east Norway. Terra Nova 17, 250-258.

Bowring, S., Myrow, P., Landing, E., Ramezani, J., Grotzinger, J., 2003. Geochronological constraints on terminal Neoproterozoic events and the rise of Metazoan, p. 13219.

Bowring, S.A., Grotzinger, J.P., Condon, D.J., Ramezani, J., Newall, M.J., Allen, P.A., 2007. Geochronologic constraints on the chronostratigraphic framework of the Neoproterozoic Huqf Supergroup, Sultanate of Oman. American Journal of Science 307, 1097-1145.

Calver, C.R., Black, L.P., Everard, J.L., Seymour, D.B., 2004. U-Pb zircon age constraints on late Neoproterozoic glaciation in Tasmania. Geology 32.

Campanha, G.A.C., Basei, M.S., Tassinari, C.C.G., Nutman, A.P., Faleiros, F.M., 2008. Constraining the age of the Iporanga Formation with SHRIMP U-Pb zircon: Implications for possible Ediacaran glaciation in the Ribeira Belt, SE Brazil. Gondwana Research 13, 117-125.

Carto, S.L., Eyles, N., 2012. Sedimentology of the Neoproterozoic (c. 580Ma) Squantum 'Tillite', Boston Basin, USA: Mass flow deposition in a deep-water arc basin lacking direct glacial influence. Sedimentary Geology 269-270, 1-14.

Chumakov, N.M., 2004. Climates and climate zonality of the Vendian: geological evidence.In: Vickers-Rich, P., Komarower, P. (Eds.), The Rise and Fall of the Ediacaran Biota.Geological Society of London, vol. 286. Special Publications, pp. 15–26.

Chumakov, N.M., 2007. Climates and climate zonality of the Vendian: geological evidence. Geological Society, London, Special Publications 286, 15-26.

Chumakov, N.M., 2009. The Baykonurian glaciohorizon of the Late Vendian. Stratigraphy and Geological Correlation 17, 373-381.

Chumakov, N.M., 2011. Chapter 23 Glacial deposits of the Bokson Group, East Sayan Mountains, Buryatian Republic, Russian Federation. Geological Society, London, Memoirs 36, 285.

Corkeron, M., 2007. 'Cap carbonates' and Neoproterozoic glacigenic successions from the Kimberley region, north-west Australia Sedimentology 54, 871-903.

Corkeron, M., 2008. Deposition and palaeogeography of a glacigenic Neoproterozoic succession in the east Kimberley, Australia. Sedimentary Geology 204, 61-82.

Corkeron, M.L., George, A.D., 2001. Glacial incursion on a Neoproterozoic carbonate platform in the Kimberley region, Australia. Geological Society of America Bulletin 113, 1121-1132.

Corkeron, M., 2011. Chapter 65 Neoproterozoic glacial deposits of the Kimberly Region and northwestern Northern Territory, Australia. Geological Society, London, Memoirs 36, 659.

Counts, J.W., Amos, K.J., 2016. Sedimentology, depositional environments and significance of an Ediacaran salt-withdrawal minibasin, Billy Springs Formation, Flinders Ranges, South Australia. Sedimentology 63, 1084-1123.

de Alvarenga, C.J.S., Figueiredo, M.F., Babinski, M., Pinho, F.E.C., 2007. Glacial diamictites of Serra Azul Formation (Ediacaran, Paraguay belt): Evidence of the Gaskiers glacial event in Brazil. Journal of South American Earth Sciences 23, 236-241.

Direen, N.G., Jago, J.B., 2008. The Cottons Breccia (Ediacaran) and its tectonostratigraphic context within the Grassy Group, King Island, Australia: A rift-related gravity slump deposit. Precambrian Research 165, 1-14.

Edwards M.B., 1984. Sedimentology of the Upper Proterozoic Glacial Record, Vestertana Group, Finnmark, North Norway, Norges Geologiske Undersøkelse Bulletin, vol. 394,76 p.

Etemad-Saeed, N., Hosseini-Barzi, M., Adabi, M.H., Miller, N.R., Sadeghi, A., Houshmandzadeh, A., Stockli, D.F., 2016. Evidence for ca. 560Ma Ediacaran glaciation in the Kahar Formation, central Alborz Mountains, northern Iran. Gondwana Research 31, 164-183.

Farmer, J., Vidal, G., Moczydlowska, M., Strauss, H., Ahlberg, P., Siedlecka, A., 1992. Ediacaran fossils from the Innerelv Member (late Proterozoic) of the Tanafjorden area, northeastern Finnmark. Geological Magazine 129, 181-195.

Gaucher, C., Blanco, G., Chiglino, L., Poiré, D., Germs, G.J.B., 2008. Acritarchs of Las Ventanas Formation (Ediacaran, Uruguay): Implications for the timing of coeval rifting and glacial events in western Gondwana. Gondwana Research 13, 488-501.

Germs, G.J.B., 1995. The Neoproterozoic of southwestern Africa, with emphasis on platform stratigraphy and paleontology. Precambrian Research 73, 137-151.

Germs, G.J.B., Gaucher, C., 2012. Nature and extent of a late Ediacaran (ca. 547Ma) glacigenic erosion surface in southearn Africa. South African Journal of Geology 115, 91-102.

Grotzinger, J.P., Bowring, S.A., Saylor, B.Z., Kaufman, A.J., 1995. Biostratigraphic and geochronologic constraints on early animal evolution. Science 270, 598-604.

Guan, B., Wu, R., Hambrey, M.J., Geng, W., 1986. Glacial sediments and erosional pavements near the Cambrian- Precambrian boundary in western Henan Province, China. Journal of the Geological Society, London 143, 311-323.

Hannah, J.L., Stein, H.J., Marolf, N., and Bingen, B. 2014. Climatic instability and regional glacial advances in the Late Ediacaran. In American Geophysical Union, Fall Meeting, abstract #PP43C-1493.

Hebert, C.L., Kaufman, A.J., Penniston-Dorland, S.C., Martin, A.J., 2010. Radiometric and stratigraphic constraints on terminal Ediacaran (post-Gaskiers) glaciation and metazoan evolution. Precambrian Research 182, 402-412.

Hofmann, M., Linnemann, U., Hoffmann, K.-H., Germs, G., Gerdes, A., Marko, L., Eckelmann, K., Gärtner, A., Krause, R., 2015. The four Neoproterozoic glaciations of southern Namibia and their detrital zircon record: The fingerprints of four crustal growth events during two supercontinent cycles. Precambrian Research 259, 176-188.

J. D. Inglis, R. S. D'Lemos, S. D. Samson, H. Admou, 2005. Geochronological Constraints on Late Precambrian Intrusion, Metamorphism, and Tectonism in the Anti-Atlas Mountains. The Journal of Geology 113, 439-450.

Jenkins, R.J., 2011. Billy Springs Glaciation, South Australia. In: The Geological Record of Neoproterozoic Glaciations (Eds E. Arnaud, G.P. Halverson and G. Sheilds-Zhou), Geol. Soc. London Mem., 36, 693–699.

Karaoui, B., Breitkreuz, C., Mahmoudi, A., Youbi, N., Hofmann, M., Gärtner, A., Linnemann, U., 2015. U–Pb zircon ages from volcanic and sedimentary rocks of the Ediacaran Bas Draâ inlier (Anti-

Atlas Morocco): Chronostratigraphic and provenance implications. Precambrian Research 263, 43-58.

Kawai, T., Windley, B.F., Terabayashi, M., Yamamoto, H., Isozaki, Y., Maruyama, S., 2008. Neoproterozoic glaciation in the mid-oceanic realm: An example from hemi-pelagic mudstones on Llanddwyn Island, Anglesey, UK. Gondwana Research 14, 105-114.

Kuzmichev, A., 2004. Tectonic History of the Tuva-Mongolian Massif: Early Baikalian, Late Baikalian, and Early Caledonian Stages. Probel-2000, Moscow.

Le Heron, D.P., Vandyk, T.M., Wu, G., Li, M., 2018. New perspectives on the Luoquan Glaciation (Ediacaran-Cambrian) of North China. The Depositional Record 4, 274-292.

Letsch, D., Large, S.J.E., Buechi, M.W., Winkler, W., von Quadt, A., 2018. Ediacaran glaciations of the west African Craton – Evidence from Morocco. Precambrian Research 310, 17-38.

Linnemann, U., Pidal, A.P., Hofmann, M., Drost, K., Quesada, C., Gerdes, A., Marko, L., Gärtner, A., Zieger, J., Ulrich, J., Krause, R., Vickers-Rich, P., Horak, J., 2018. A ~565 Ma old glaciation in the Ediacaran of peri-Gondwanan West Africa. International Journal of Earth Sciences 107, 885-911.

Maslov, A.V., Meert, J., Levashova, N.M., Ronkin, Y.L., Grazhdankin, D.V., Kuznetsov, N.B., Krupenin, M.T., Fedorova, N.M., Ipat'eva, I.S., 2013. New constraints for the age of Vendian glacial deposits (Central Urals). Doklady Earth Sciences 449, 303-308.

McCay, G.A., Prave, A.R., Alsop, G.I., Fallick, A.E., 2006. Glacial trinity: Neoproterozoic Earth history within the British-Irish Caledonides. Geology 34.

McGee, B., Collins, A.S., Trindade, R.I.F., 2013. A Glacially Incised Canyon in Brazil: Further Evidence for Mid-Ediacaran Glaciation? The Journal of Geology 121, 275-287.

McGee, B., Collins, A.S., Trindade, R.I.F., Payne, J., 2015. Age and provenance of the Cryogenian to Cambrian passive margin to foreland basin sequence of the northern Paraguay Belt, Brazil. GSA Bulletin 127, 76-86.

Nystuen J.,1976. Late Precambrian Moelv tillite deposited on a discontinuity surface associated with a fossil ice wedge, Rendalen, southern Norway Norsk Geologiske Tidsskrift, 56, pp. 29-50

Osokin, P.V., Tyzhinov, A.V., 1998. Precambrian tilloids of the Oka-Khubsugul phosphorite-bearing basin (eastern Sayan, northwestern Mongolia). Lithol. Miner. Resour. 33, 142-154.

Oyhantçabal, P., Siegesmund, S., Wemmer, K., Naumann, R., 2006. Age and geochemical signature of post-collisional plutons of the southern extreme of the Dom Feliciano Belt (Uruguay). V. South American Symposium on Isotope Geology, Short Papers, Punta del Este, p. 148.

Pang, K., Wu, C., Sun, Y., Ouyang, Q., Yuan, X., Shen, B., Lang, X., Wang, R., Chen, Z., Zhou, C., 2021. New Ediacara-type fossils and late Ediacaran stratigraphy from the northern Qaidam Basin (China): Paleogeographic implications. Geology.

Piacentini, T., Vasconcelos, P.M., Farley, K.A., 2013. 40Ar/39Ar constraints on the age and thermal history of the Urucum Neoproterozoic banded iron-formation, Brazil. Precambrian Research 228, 48-62.

Pu, J.P., Bowring, S.A., Ramezani, J., Myrow, P., 2016. Dodging snowballs: Geochronology of the Gaskiers glaciation and the first appearance of the Ediacaran biota. Geology (Boulder) 44, 955-958.

Rice, A.H.N., Edwards, M.B., Hansen, T.A., Arnaud, E., Halverson, G.P., 2011. Glacigenic rocks of the Smalfjord and Mortensnes formations, Vestertana Group, E. Finnmark, Norway. In: Arnaud, E, Shields, G., Halverson, G.P. (eds.), The Geological Record of Neoproterozoic Glaciations, Geological Society of London Memoir 36, 593–602

Sayles, R.W., 1914. The Squantum Tillite. Bulletin of the Museum of Comparative Zoology at Harvard College 56, 141-175, 12 plates, Cambridge, MA.

Shen, B., Xiao, S., Zhou, C., Kaufman, A.J., Yuan, X., 2010. Carbon and sulfur isotope chemostratigraphy of the Neoproterozoic Quanji Group of the Chaidam Basin, NW China: Basin stratification in the aftermath of an Ediacaran glaciation postdating the Shuram event? Precambrian Research 177, 241-252.

Silva, L.J.H.D.e.-R., Walde, D.H.-G., Saldanha, D.O., 2016. The Neoproterozoic–Cambrian Paraguay Belt, central Brazil: Part I — New structural data and a new approach on the regional implications. Tectonophysics 676, 20-41.

Southworth, S., Tollo, R.P., Aleinikoff, J.N., Bailey, C., Burton, W.C., Crider, E., Hackley, P.C., Kunk, M.J., Mundil, R., Naeser, C.N., Naeser, N., and Smoot, J., 2009. New geologic map and geochronology of the Shenandoah National Park region, Virginia. Geological Society of America Abstracts with Programs 41, 365.

Thompson, M.D., Bowring, S.A., 2000. Age of the Squantum 'tillite', Boston basin, Massachusetts: U-Pb zircon constraints on terminal Neoproterozoic glaciation. American Journal of Science 300, 630-655.

Vernhet, E., Youbi, N., Chellai, E.H., Villeneuve, M., El Archi, A., 2012. The Bou-Azzer glaciation: Evidence for an Ediacaran glaciation on the West African Craton (Anti-Atlas, Morocco). Precambrian Research 196-197, 106-112.

Vickers-Rich P, Fedonkin MA, 2007. The proterozoic (2.5 billion to 542 million years ago). In: Fedonkin MA, Gehling JG, Grey K, Narbonne GM, Vickers-Rich P (eds) The rise of animals. The Johns Hopkins University Press, Baltimore, pp 29–51

Walter, M.R., Veevers, J.J., Calver, C.R., Gorjan, P., Hill, A.C., 2000. Dating the 840–544 Ma Neoproterozoic interval by isotopes of strontium, carbon, and sulfur in seawater, and some interpretative models. Precambrian Research 100, 371-433.

Xiao, S., 2004. Neoproterozoic glaciations and biological evolution: Data from the Tarim and Yangtze blocks, China, in: Reimold, W.U., Hofmann, A. (Eds.), Abstract Volume of GSA/GSSA Field Forum "Processes on the Early Earth", p. 99.

Xu, B., Xiao, S., Zou, H., Chen, Y., Li, Z., Song, B., Liu, D., Zhou, C., Yuan, X., 2009. SHRIMP zircon U–Pb age constraints on Neoproterozoic Quruqtagh diamictites in NW China. Precambrian Research 168, 247-258.

References (Table S4):

Halls, H.C., Lovette, A., Hamilton, M., Söderlund, U., 2015. A paleomagnetic and U–Pb geochronology study of the western end of the Grenville dyke swarm: Rapid changes in paleomagnetic field direction at ca. 585Ma related to polarity reversals? Precambrian Research 257, 137-166.

Huang, B., Yang, Z., Otofuji, Y.-i., Zhu, R., 1999. Early Paleozoic paleomagnetic poles from the western part of the North China Block and their implications. Tectonophysics 308, 377-402.

Hyodo, H., Dunlop, D.J., 1993. Effect of anisotropy on the paleomagnetic contact test for a Grenville Dike. Journal of Geophysical Research: Solid Earth 98, 7997-8017.

Jing, X., Yang, Z., Tong, Y., Wang, H., Xu, Y., 2018. Identification of multiple magnetizations of the Ediacaran strata in South China. Geophysical Journal International 212, 54-75.

Kravchinsky, V.A., Konstantinov, K.M., Cogné, J.P., 2001. Palaeomagnetic study of Vendian and Early Cambrian rocks of South Siberia and Central Mongolia: was the Siberian platform assembled at this time? Precambrian Research 110, 61-92.

Levashova, N.M., Bazhenov, M.L., Meert, J.G., Danukalov, K.N., Golovanova, I.V., Kuznetsov, N.B., Fedorova, N.M., 2015. Paleomagnetism of upper Ediacaran clastics from the South Urals: Implications to paleogeography of Baltica and the opening of the Iapetus Ocean. Gondwana Research 28, 191-208.

Lubnina, N.V., Pisarevsky, S.A., Puchkov, V.N., Kozlov, V.I., Sergeeva, N.D., 2014. New paleomagnetic data from Late Neoproterozoic sedimentary successions in Southern Urals, Russia: implications for the Late Neoproterozoic paleogeography of the Iapetan realm. International Journal of Earth Sciences 103, 1317-1334.

McCausland, P.J.A., Hankard, F., Van der Voo, R., Hall, C.M., 2011. Ediacaran paleogeography of Laurentia: Paleomagnetism and 40Ar–39Ar geochronology of the 583Ma Baie des Moutons syenite, Quebec. Precambrian Research 187, 58-78.

McNamara, A.K., Niocaill, C.M., van der Pluijm, B.A., der Voo, R.V., 2001. West African proximity of the Avalon terrane in the latest Precambrian. Geological Society of America Bulletin 113, 1161.

Meert, J.G., Van der Voo, R., Payne, T.W., 1994. Paleomagnetism of the Catoctin volcanic province: A new Vendian-Cambrian apparent polar wander path for North America. Journal of Geophysical Research: Solid Earth 99, 4625-4641.

Mills, A.J., Dunning, G.R., Murphy, M., Langille, A., 2017. New geochronological constraints on the timing of magmatism for the Bull Arm Formation, Musgravetown Group, Avalon Terrane, northeastern Newfoundland. Current Research (2017) Newfoundland and Labrador Department of Natural Resources Geological Survey, Report 17-1, 1-17.

Mitchell, R.N., Evans, D.A.D., Kilian, T.M., 2010. Rapid Early Cambrian rotation of Gondwana. Geology 38, 755-758.

Murthy, G.S., 1971. The Paleomagnetism of Diabase Dikes from the Grenville Province. Canadian Journal of Earth Sciences 8, 802.

Pisarevsky, S.A., McCausland, P.J.A., Hodych, J.P., O'Brien, S.J., Tait, J.A., Murphy, J.B., Colpron, M., 2012. Paleomagnetic study of the late Neoproterozoic Bull Arm and Crown Hill formations (Musgravetown Group) of eastern Newfoundland: implications for Avalonia and West Gondwana paleogeography1This article is one of a series of papers published in CJES Special Issue:

In honour of Ward Neale on the theme of Appalachian and Grenvillian geology. Canadian Journal of Earth Sciences 49, 308-327.

Robert, B., Besse, J., Blein, O., Greff-Lefftz, M., Baudin, T., Lopes, F., Meslouh, S., Belbadaoui, M., 2017. Constraints on the Ediacaran inertial interchange true polar wander hypothesis: A new paleomagnetic study in Morocco (West African Craton). Precambrian Research 295, 90-116.

Robert, B., Greff-Lefftz, M., Besse, J., 2018. True Polar Wander: A Key Indicator for Plate Configuration and Mantle Convection During the Late Neoproterozoic. Geochemistry, Geophysics, Geosystems 19, 3478-3495.

Schmidt, P.W., Williams, G.E., 2010. Ediacaran palaeomagnetism and apparent polar wander path for Australia: no large true polar wander. Geophysical Journal International 182, 711-726.

Sparkes, G., Dunning, G., 2014. Late Neoproterozoic epithermal alteration and mineralization in the western Avalon zone: a summary of mineralogical investigations and new u/pb geochronological results. Current Research (2014) Newfoundland and Labrador Department of Natural Resources, Geological Survey, Report 14-1, 99-128.

Symons, D.T.A., Chiasson, A.D., 1991. Paleomagnetism of the Callander Complex and the Cambrian apparent polar wander path for North America. Canadian Journal of Earth Sciences 28, 355.

Tanczyk, E.I., Lapointe, P., Morris, W.A., Schmidt, P.W., 1987. A paleomagnetic study of the layered mafic intrusion at sept-hes, Quebec1. Can. J. Earth Sci. 24, 1431-1438.

Thompson, M.D., Grunow, A.M., Ramezani, J., 2007. Late Neoproterozoic paleogeography of the Southeastern New England Avalon Zone: Insights from U-Pb geochronology and paleomagnetism. Geological Society of America Bulletin 119, 681-696.

Wen, B., Evans, D.A.D., Anderson, R.P., McCausland, P.J.A., 2020. Late Ediacaran paleogeography of Avalonia and the Cambrian assembly of West Gondwana. Earth and Planetary Science Letters 552, 116591.

Zhao, H., Zhang, S., Zhu, M., Ding, J., Li, H., Yang, T., Wu, H., 2020. Paleomagnetic insights into the Cambrian biogeographic conundrum: Did the North China craton link Laurentia and East Gondwana? Geology 49, 372-376.

Zhao, P., Chen, Y., Zhan, S., Xu, B., Faure, M., 2014. The Apparent Polar Wander Path of the Tarim block (NW China) since the Neoproterozoic and its implications for a long-term Tarim–Australia connection. Precambrian Research 242, 39-57.

Zhu, B., Becker, H., Jiang, S.-Y., Pi, D.-H., Fischer-Gödde, M., Yang, J.-H., 2013. Re–Os geochronology of black shales from the Neoproterozoic Doushantuo Formation, Yangtze platform, South China. Precambrian Research 225, 67-76.